ARTICLE

https://doi.org/10.1590/2317-4889202220220017

BJGEO
Brazilian Journal of Geology

Neoarchean to Rhyacian crustal records along the Middle Xingu River area, Amazonian craton

Moacir José Buenano Macambira[1]*, Marcelo Lacerda Vasquez[2], Pablo Conduru Monteiro[3], Richard Austin Armstrong[4]

Abstract

The Carajás (3.0–2.5 Ga) and Xingu-Iricoumé (1.99–1.86 Ga) blocks comprise the Central Amazonia Province (CAP) that is in contact with the Maroni-Itacaiúnas Province (MIP) within the Amazonian craton. The CAP is the oldest portion (Nd-T_{DM}) of the craton and corresponds to an Archean nucleus bordered by younger Paleo-Mesoproterozoic mobile belts, including the MIP. Because the location and tectonic boundaries between these provinces are insufficiently known, we carried out a geological survey along the Middle Xingu River, cutting the WNW-ESE regional trend, to further understand cratonic evolution of the MIP and its southeastern boundary in this key area. Geochronologic results (Pb-evaporation and U-Pb SHRIMP in zircon and monazite), supported by petrographic and field observations, allowed identification of the following lithotypes and their ages: migmatitic gneisses (2859–2080 Ma), tonalitic gneisses (2554 ± 3 Ma, 2480 ± 9 Ma), enderbites (2114 ± 3 Ma), charnockites (2094 ± 4 Ma, 2084 ± 2 Ma), granodiorites (2079 ± 3 Ma), leucogranitic vein (2075 ± 2 Ma), and pelitic paragneisses (2062 ± 8 Ma). These ages are related to the reworking of Archean crust during Rhyacian magmatic arc amalgamation (2.22–2.13 Ga) and collision in the Transamazonian cycle (*ca.* 2.1 Ga).

KEYWORDS: Transamazonian cycle; Maroni-Itacaiúnas Province; Amazonian craton; Zircon and monazite geochronology.

INTRODUCTION

The boundaries between the geochronological provinces that form the Amazonian craton (Fig. 1A, Cordani *et al.* 1979, Teixeira *et al.* 1989, Tassinari and Macambira 2004), in northern South America, represent key areas to understand the differences in age and tectonic episodes that built the craton. However, such areas are often poorly known in terms of their extension and nature. In the southeastern Amazonian craton, the border region between the Central Amazonia Province (CAP), considered an Archean nucleus, and the surrounded Maroni-Itacaiúnas Province (MIP, 2.2–1.95 Ga) is highlighted. The rocks of the MIP are formed by Archean to Rhyacian rocks, which are strongly affected by the Transamazonian cycle, and present world-scale correlative orogenesis such as the Birimian in western Africa (e.g., Ledru *et al.* 1994, Grenholm 2019).

Tassinari and Macambira (1999) divided the CAP into the Archean Carajás block and the Xingu-Iricoumé block. The last one is dominated by Paleoproterozoic rocks generated by crustal reworking of Archean material (Nd-T_{DM} > 2.5 Ga). The Bacajá domain marks the southern boundary of the MIP with the Carajás block and is limited by the Xingu-Iricoumé block to the west/southwest (Fig. 1A). The boundary between these blocks roughly follows the middle course of the Xingu River. This river transversally cuts the main structures of the western Bacajá domain; hence, it constitutes an excellent way to investigate the geology of this domain and its border (Fig. 2). Additionally, there are few roadways in this dense rainforest region.

To improve the geological mapping and refine the evolution of the MIP and its boundaries with the CAP, the southwestern sector of the Bacajá domain — a typical Rhyacian terrain related to the evolution of the Transamazonian cycle — was investigated through field, petrographic, and geochronological studies (Pb-evaporation and U-Pb sensitive high-resolution ion microprobe [SHRIMP] applied to zircon and monazite).

[1]Laboratório de Geologia Isotópica, Instituto de Geociências, Universidade Federal do Pará – Belém (PA), Brazil. E-mail: moamac@ufpa.br

[2]Serviço Geológico do Brasil – Belém (PA), Brazil. E-mail: marcelo-vasquez@cprm.gov.br

[3]Programa de Pós-Graduação em Geologia e Geoquímica, Instituto de Geociências, Universidade Federal do Pará – Belém (PA), Brazil.

[4]Research School of Earth Science, Australian National University – Canberra, Australia. E-mail: richard.armstrong@anu.edu.au

*Corresponding author.

REGIONAL GEOLOGY

The Amazonian craton was divided by the Amazon basin into the northern Guiana Shield and the southern Central Brazil Shield (e.g., Almeida *et al.* 1981) (Fig. 1B). According to its current evolutionary model, the craton consists of an Archean nucleus into which Proterozoic belts or magmatic arcs were amalgamated in the north-northeast and southwest directions due to episodic events of reworking and/or juvenile crustal growth. Having interior similarity in the geological record and age, these regions constitute geochronological provinces

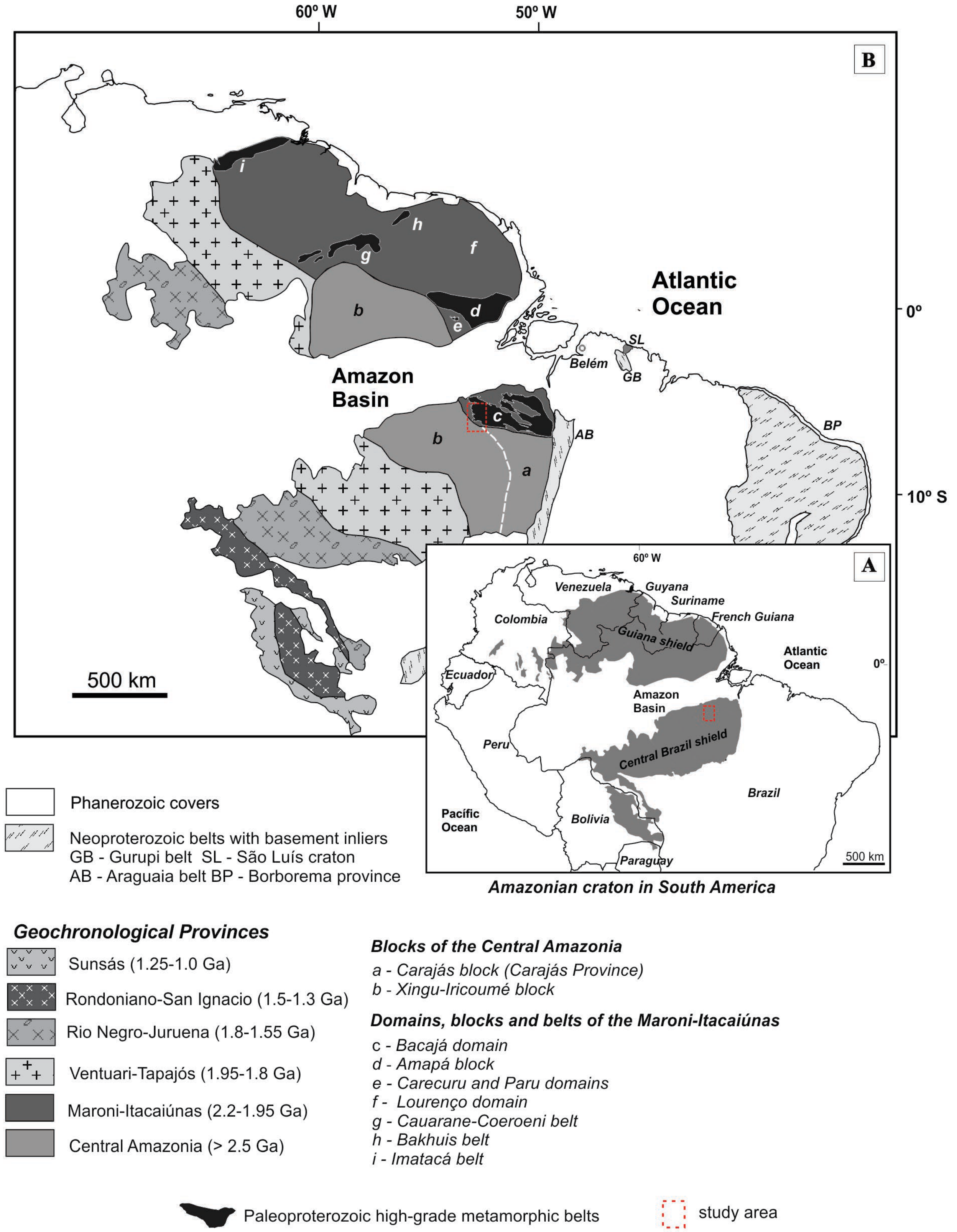

Figure 1. Sketch map of geochronological provinces from the Amazonian craton (modified after Tassinari and Macambira 2004). (A) Shields of Amazonian craton. (B) Geochronological provinces with tectonic domains, blocks, and Paleoproterozoic high-grade metamorphic belts from eastern part of the craton and the study area.

subjected to different geographical and geological environments (Cordani *et al.* 1979, Teixeira *et al.* 1989, Tassinari *et al.* 2000, Santos *et al.* 2000, Tassinari and Macambira 1999, 2004). In the model proposed by Tassinari and Macambira (2004), which follows previous authors, the Amazonian craton is divided into six main geochronological provinces (Fig. 1A).

Outcrops of Paleoproterozoic granitoids (1.96–1.92 Ga), the ones of volcano-plutonic rocks (1.88–1.81 Ga), and the Nd-T_{DM} ages of 2.5–3.1 Ga found for the western portion and, supposedly, the northern portion of the CAP, led Tassinari and Macambira (1999) to classify the province into two areas (Fig. 1). The first one is composed of Paleoproterozoic

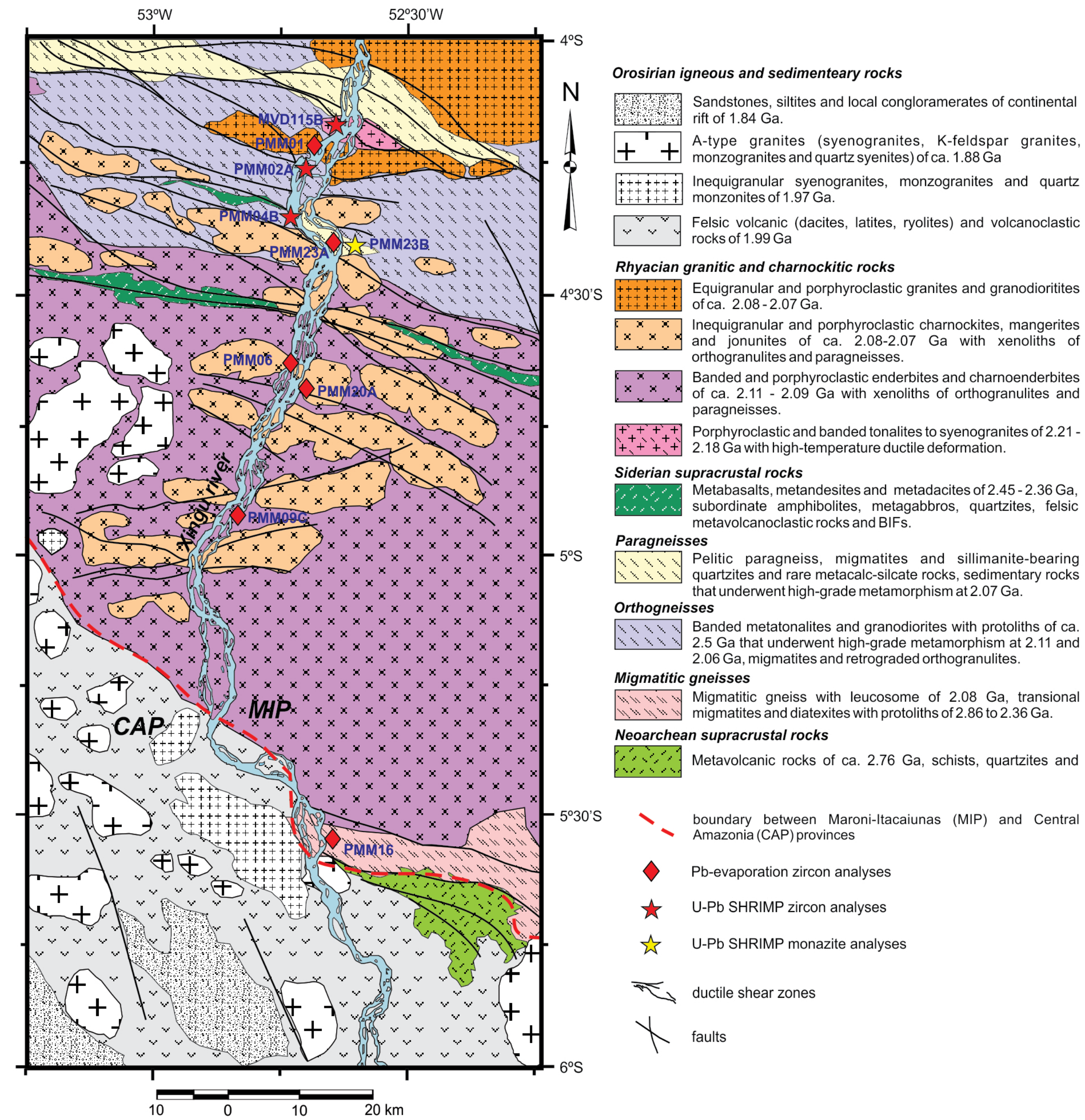

Source: modified from Vasquez *et al.* (2008b).
Figure 2. Sketch geological map of Middle Xingu River area of the Bacajá domain and dating samples.

igneous and sedimentary rocks (Xingu-Iricoumé block) with an Archean heritage (inherited zircon or Nd-T_{DM}), and the second one is composed of an Archean basement (Carajás block). In the southern portion of the Xingu-Iricoumé block, there are outcrops of felsic volcanic rocks and granites with zircon U-Pb and Pb-evaporation ages between 1.99 and 1.86 Ga (e.g., Alves *et al.* 2010, Fernandes *et al.* 2011, Semblano *et al.* 2016) covered by Paleoproterozoic (< 1.84 Ga) epiclastic sedimentary rocks. In the boundary regions, the igneous rocks of ca. 1.88 Ga and the associated epiclastic sedimentary rocks cut and cover Archean (3.0–2.5 Ga) and early Paleoproterozoic (probably Siderian and Rhyacian) rocks of Carajás block as well as Orosirian rocks (2.03–1.96 Ga) of Venturi-Tapajós Province (Vasquez *et al.* 2008b).

The boundary between the Carajás block of CAP and the southeastern part of MIP (Bacajá domain, Fig. 1A) was proposed by Cordani *et al.* (1984) who, based on Rb-Sr and K-Ar geochronological data, marked a tentative boundary approximately along latitude 6°S to distinguish the Archean rocks of the Carajás block from the Paleoproterozoic ones in the north, in MIP. In addition to values close to 2.0 Ga, amphibole K-Ar data indicating amphibolites of this area are about 2.5 Ga old suggest the presence of reworked Archean segments. Based on Rb-Sr data of paragneisses and metabasic rocks, Santos *et al.* (1988) identified crustal accretion in ca. 2.0 Ga and reworking of older rocks in the southwestern portion of MIP. Subsequently, zircon Pb-evaporation and U-Pb ages and Sm-Nd data confirmed that the Paleoproterozoic evolution of the Bacajá domain involved the reworking of Archean crustal segments (3.0–2.5 Ga) as well as the juvenile crust formation in Siderian (2.49–2.44 and 2.36–2.31 Ga) and Rhyacian (2.21–2.05 Ga) times (Santos 2003, Faraco *et al.* 2005, Vasquez *et al.*

2005, 2008a, 2008b, Macambira *et al.* 2009). In contrast, the geochronological data have shown that Mesoarchean (3.0–2.97 Ga) rocks of the northern Carajás block were reworked in about 2.85 Ga, and mafic-ultramafic and granitic plutonic bodies were emplaced in 2.78–2.74 Ga with local intrusions in ca. 2.5 Ga (Olszewski *et al.* 1989, Machado *et al.* 1991, Macambira and Lafon 1995, Barros *et al.* 2004, Moreto *et al.* 2011, Feio *et al.* 2013).

According to zircon ages and Nd-isotope data, the evolution of the Bacajá domain can be summarized in the following chronological order:

- Formation of tonalites to granites between 3.0 and 2.67 Ga in the northern, central, and southern portions of the domain with emplacement of juvenile rocks in 2.7 Ga (Nd-T_{DM} = 2.7 Ga; $\varepsilon Nd_{(t)}$ = 2.7; Macambira *et al.* 2009) in the central portion, which may be related to an early island arc (Vasquez *et al.* 2008a, 2008b);
- Emplacement of tonalites to granites between 2.50 and 2.34 Ga from Archean sources (Nd-T_{DM} = 2.9 Ga; $\varepsilon Nd_{(t)}$ = -2.9; Macambira *et al.* 2009);
- Deposition of volcano-sedimentary sequences with basalts and andesites of an island arc (Besser 2012) with crystallization age of 2.4 Ga (Nd-T_{DM} = 2.58–2.7 Ga; $\varepsilon Nd_{(t)}$ = 0.78 to -0.71; Macambira *et al.* 2009);
- Emplacement of quartz monzodiorites to granites between 2.22 and 2.13 Ga related to continental margin arc (Nd-T_{DM} = 2.9–2.4 Ga; $\varepsilon Nd_{(t)}$ = -7.6 to +0.2; Vasquez *et al.* 2008a, 2008b, Macambira *et al.* 2009);
- High-grade metamorphism in *ca*. 2.1 Ga with the reworking of Archean (3.0–2.6 Ga), Siderian (2.5–2.34 Ga), and Rhyacian (2.22–2.13 Ga) rocks during continental collision (Macambira *et al.* 2007, Vasquez *et al.* 2008b);
- Emplacement of charnockitic and granitic rocks between 2.11 and 2.07 Ga in syn- to post-collisional settings (Macambira *et al.* 2007, Vasquez *et al.* 2008a, 2008b).

LOCAL GEOLOGY

The Middle Xingu River area is situated in the southwestern part of the Bacajá domain, which is a key area for studying the boundary between MIP and CAP (Fig. 1A). In the southwestern part of this area, Paleoproterozoic rocks of the Xingu-Iricoumé block outcrop, whereas Archean rocks of the Carajás block outcrop in the southeastern part (Fig. 2).

The Middle Xingu River area is only accessed by the Xingu River which crosscuts the WNW-ESE trend of igneous and metamorphic rocks of the Bacajá domain (Fig. 2). Previous geological surveys in this area mapped migmatites, ortho- and paragneisses, supracrustal rocks (greenstone belts), granites, and local granulites (e.g., Jorge João *et al.* 1987, Santos *et al.* 1988). Charnockitic rocks and granulite belts were mapped in the western and southern portions of the Bacajá domain (Vasquez *et al.* 2008a, 2008b). Field descriptions and petrographic study of outcrops along the Middle Xingu River allowed distinguishing migmatitic gneisses, orthogneisses, pelitic paragneisses, charnockitic, and granitic rocks (Fig. 2).

Orthogneisses

In the northern portion of the study area (Fig. 2), there are outcrops of banded metatonalites and metagranodiorites with leucogranitic veins (Fig. 3A). Sometimes these outcrops are just foliated with stretched mafic granular enclaves (Fig. 3B). These orthogneisses show hornblende and biotite in a polygonal granoblastic quartz feldspathic matrix (Figs. 3C and 3D), which indicates high-temperature recrystallization (> 550°C, Passchier and Trouw 2005). However, this recrystallization was overprinted by low-temperature recrystallization (< 550°C, Passchier and Trouw 2005), as indicated by the fine recrystallization bands (Fig. 3C). Orthogranulites and retrograded orthogranulites (orthogneisses) were mapped in a WNW-ESE high-grade metamorphic belt of the Bacajá domain (Vasquez *et al.* 2008c, Macambira and Ricci 2013, Macambira *et al.* 2016). Santos *et al.* (1988) mapped migmatites with dominant leucosome in this area, but only a few leucosome migmatitic orthogneisses were mapped in our survey.

Paragneisses

The WNW-ESE paragneiss belts outcrop in the northern area of the Middle Xingu River (Fig. 2). These rocks are sillimanite-cordierite-garnet-biotite gneisses to garnet-biotite gneisses. This mineral assemblage indicates pelitic protoliths for these paragneisses (Bucher and Grapes 2011), but Santos *et al.* (1988) also mapped local calciosilisiclaste protoliths. These paragneisses show migmatitic structures as leucosome pockets with centimetric porphyroblasts of garnet (Figs. 3E and 4A) and leucogranitic veins with cordierite and red biotite (Figs. 4B and 3F). The pelitic paragneisses host mafic granulite boudins (Fig. 3F), which were basic rocks (lavas or dykes) associated with pelitic sedimentary rocks. A pelitic paragneiss (PMM-23B) and a leucogranitic vein (PMM-23A), which correspond to the leucosome of this migmatitic paragneiss, were selected for geochronological study.

Migmatic gneisses

Santos *et al.* (1988) mapped rich schollen and schlieren metatexites that correspond to the transitional migmatites of Sawyer (2008), in the southeastern area of Middle Xingu River. In the present survey, diatexites with schlieren (Fig. 4C) together with metatexites with subordinated gneisses and amphibolites were mapped. The leucosome shows porphyroclastic K-feldspar in a polygonal granoblastic quartz feldspathic matrix, indicating high-temperature recrystallization overprinted by low-temperature recrystallization bands (Fig. 4D), which indicates retrograde metamorphism. A leucosome of migmatitic gneiss was selected for geochronology (PMM-16). It is not possible to distinguish if the protolith of this migmatitic gneiss was ortho- or paraderived.

Charnockitic rocks

In the central part of the Middle Xingu River area, enderbites and charnoenderbites (Fig. 2) with porphyroclastic (Fig. 4E) and inequigranular (Fig. 4F) textures are outcropping. Sometimes they show igneous banding, mingling with mafic

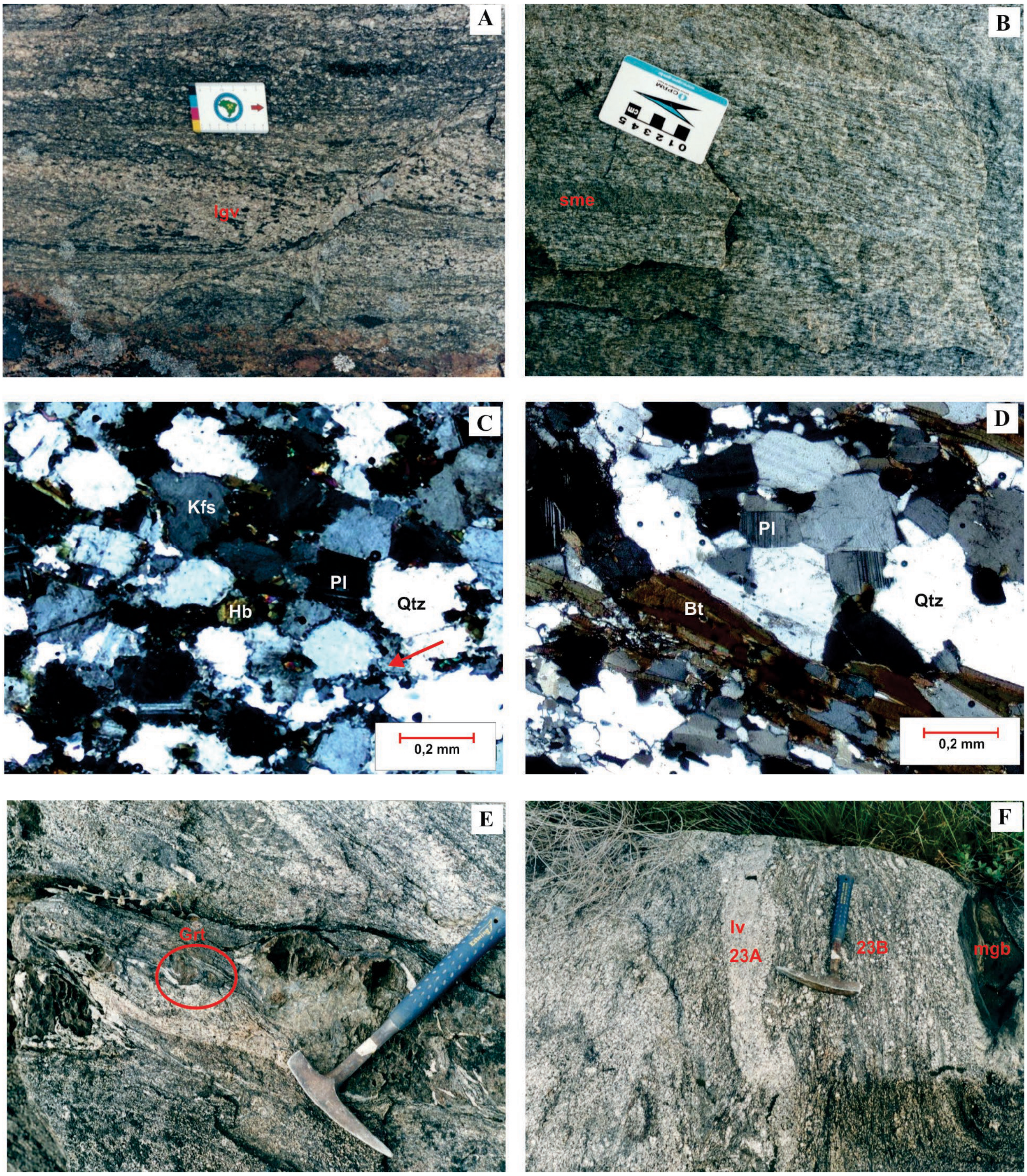

Figure 3. Mesoscopic structures and microtextures of orthogneisses and paragneisses. (A) Leucogranitic vein (lgv) in metatonalite. (B) Strechted mafic enclave (sme) in foliated metatonalite. (C) Polygonal granoblastic matrix of plagioclase (Pl), hornblende (Hb), K-feldspar (Kfs) and quartz (Qtz), and fine recrystallized bands - red arrow (sample PMM-02A). (D) Polygonal granoblastic matrix of plagioclase, biotite (Bt) and quartz (sample PMM-04B). (E) Porphyroblasts of garnet (Grt) in leucosome pocket. (F) Leucogranitic vein (lv) (sample PMM-23A) and mafic granulite boudin (mgb) in pelitic paragneiss (sample PMM-23B). Microscopic images took in crossed polarized light. In figure A, scale is 8.5 cm long. In figures E and F, hammerhead is 18 cm long.

magmas, xenoliths of orthogranulite (Fig. 4E), and clusters of hornblende and pyroxene (Fig. 4F). Coarse-grained inequigranular charnockites bodies (Fig. 5A) are oriented to WNW-ESE and E-W cut enderbites and charnoenderbites, as well as ortho- and paragneisses (Fig. 2). Both types of charnockitic rocks have mesopertites (Fig. 5B), antipertites (Fig. 5C), and orthopyroxene and clinopyroxene relics (Fig. 5D). An enderbite (PMM-09C) and two charnockites (PMM-06 and PMM-20) were selected for geochronology.

Granitic rocks

A pluton of porphyroclastic monzogranite of 2147 ± 5 Ma (Vasquez *et al.* 2008a) cuts ortho- and paragneisses of the northern portion of the study area (Fig. 2). This granitic body was intruded by equigranular granodiorite (Fig. 5E) with low-temperature recrystallization rims of plagioclase, K-feldspar, and quartz (Fig. 5F). Similar granitic bodies outcrop in the northeastern portion of the Middle Xingu River (Fig. 2). A sample of this granodiorite (PMM-01) was selected for geochronology.

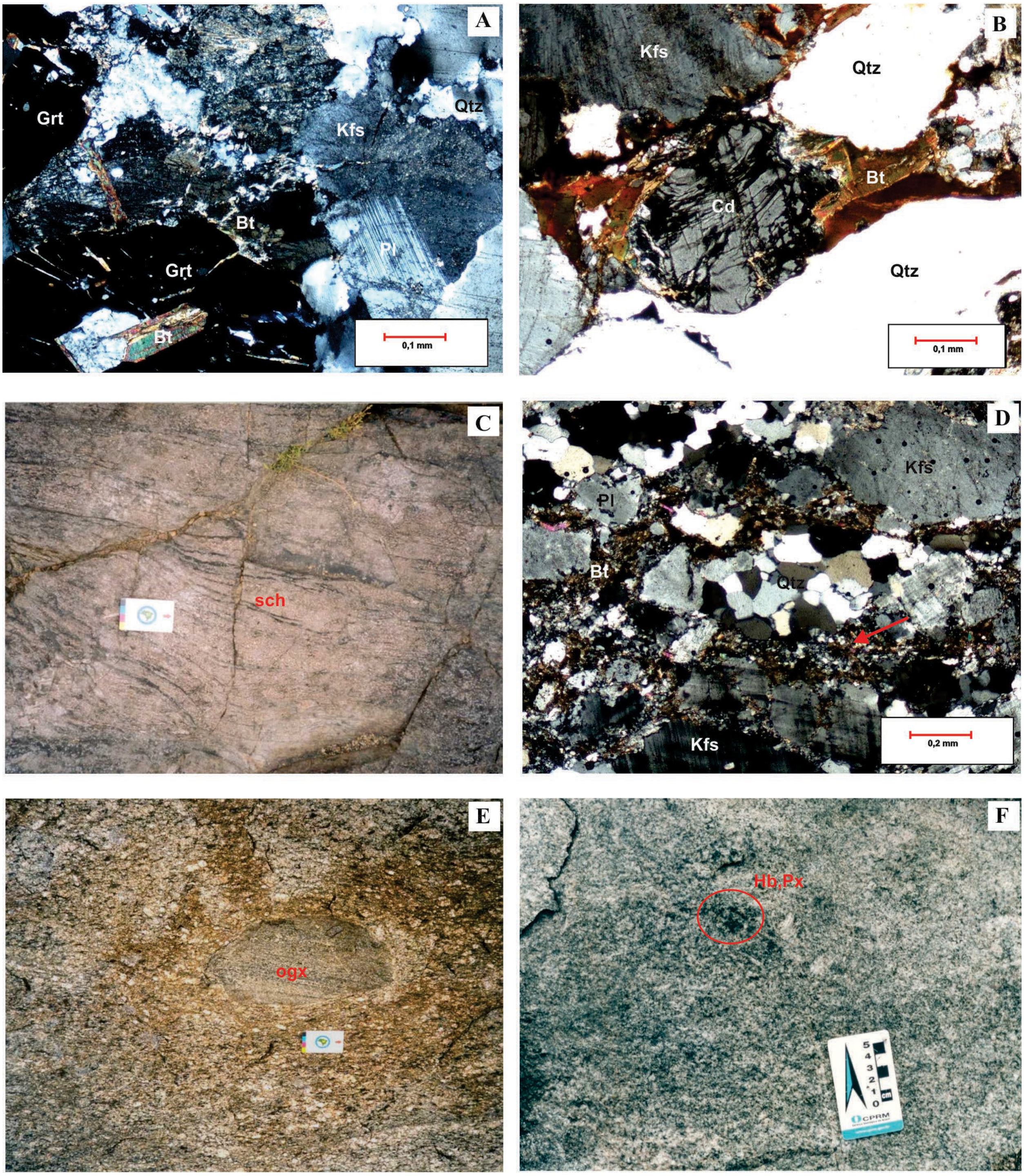

Figure 4. Mesoscopic structures and microtextures of paragneisses, migmatites and enderbites. (A) Porphyroblasts of garnet with biotite, plagioclase, K-feldspar and quartz. (B) Cordierite (Cd), biotite, K-feldspar and quartz in pelitic paragneiss (sample PMM-23B). (C) Schlierens (sch) in leucosome pocket (pink) in migmatitic gneiss (grey). (D) Porphyroclasts of K-feldspar in polygonal granoblastic matrix and fine recrystallized bands rich in biotite - red arrow - in leucosome (sample PMM-16). (E) Orthogranulite xenolith (ogx) in foliated enderbite. (F) Mafic clusters of hornblende (Hb) and pyroxenes (Px) in inequigranular enderbite (sample PMM-09C). Microscopic images took in crossed polarized light. In figures C and E, scale is 8.5 cm long.

Other units

In the southeastern portion of the study area, Neoarchean supracrustal rocks of the Carajás block of CAP (e.g., Vasquez *et al.* 2008b) are outcropping (Fig. 2). In the southwestern portion, felsic volcanic and volcanoclastic rocks of 1.99 Ga, cut by granites of 1.97 Ga and A-type granites of 1.88 Ga (Alves *et al.* 2010, Semblano *et al.* 2016) of the Xingu-Iricoumé block, cover, and cut migmatitic gneisses and charnockitic rocks of Bacajá domain of MIP (Fig. 2).

ZIRCON GEOCHRONOLOGY

Methodology

Dating of zircon was undertaken using the single zircon Pb-evaporation and the U–Pb SHRIMP methods. Pb-evaporation was carried out at the Isotope Geology Laboratory (Para-Iso) of the Federal University of Pará, Brazil, where zircon concentrates were obtained by gravimetric (elutriation and heavy liquids) and magnetic (isodynamic separator)

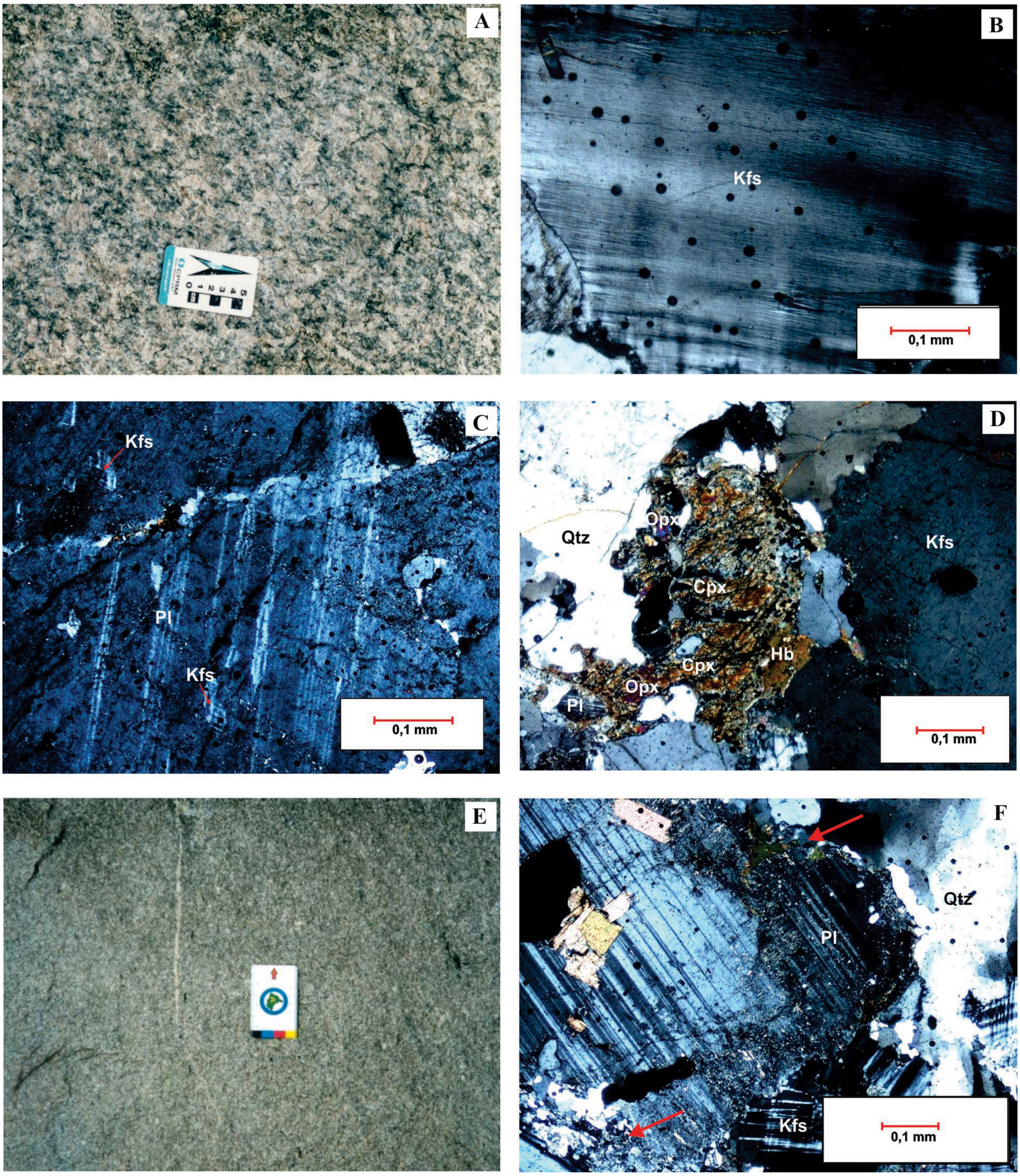

Figure 5. Mesoscopic structures and microtextures of charnockites and granodiorites. (A) Coarsed-grained charnockite. (B) Mesoperthite in porphyroclast of K-feldspar. (C) Antiperthite (K-feldspar drop) in plagioclase. (D) orthopyroxene (Opx) and clinopyroxene (Cpx) relics in chanockites. (E) Equigranular granodiorite with (F) crystals of plagioclase, K-feldspar and quartz with rims of recrystallized bands - red arrows (sample PMM-01). Microscopic images took in crossed polarized light. In figure E, scale is 8.5 cm long.

techniques. Grains were selected for analysis by handpicking under the stereomicroscope.

Single Zircon Pb-evaporation

The method of Pb-evaporation from zircon monocrystals, advocated by Kober (1986), was undertaken using the ion-counting system of a Finnigan MAT 262 mass spectrometer in dynamic mode at the Para-Iso Laboratory. Two facing Re filaments were employed; one containing zircon for evaporation and another for Pb ionization, from which isotopes are analyzed. Three evaporation steps at 1,450, 1,500, and 1,550°C are usually performed to reach different levels of Pb extraction. For each evaporation step, up to five isotopic ratio blocks are obtained in a monocollector. The average $^{207}Pb/^{206}Pb$ ratio of the blocks defines the corresponding age for each extraction step. In the case of coinciding ages, an average is calculated for each grain. Otherwise, when steps yield in discrepant/usually lower ages, the blocks are discarded for each grain (subjective elimination). Blocks and steps yielding $^{204}Pb/^{206}Pb > 0.0004$ are also discarded to prevent initial Pb correction, which is obtained by comparison with the two-stage terrestrial Pb evolution model (Stacey and Kramers 1975). The average age is calculated again from several grains of the same sample in order to eliminate outlying values. Results are filtered and statistically treated according to the Para-Iso routine (Gaudette *et al.* 1998). Pb-evaporation ages are expressed in 2σ confidence intervals.

U-Pb SHRIMP in zircon and monazite

U-Pb analyses were undertaken on a SHRIMP at the Research School of Earth Sciences of the Australian National University in Canberra, Australia. Zircon and monazite grains were mounted in epoxy resin together with respective standard grains (SL13 and FC1 zircons, Thompson mine monazite). Cathodoluminescence (CL) and backscattered electron (BSE) images were obtained by scanning electron microscopy to see the internal structures, microfractures, and damage zones, respectively, of zircon and monazite crystals and selected sites for analysis. SHRIMP analytical procedures were applied according to the methods described by Compston *et al.* (1984) and Williams (1998). Raw isotopic data were reduced using the Squid program (Ludwig 2001), whereas age calculations and Concordia plots were performed using both the Squid and Isoplot software (Ludwig 2003). Analyses and ages for individual SHRIMP spots are presented with 1σ uncertainties. When data are combined to calculate an age, the quoted uncertainties are at a 95% confidence level with uncertainties in the U-Pb standard calibration included in any relevant U-Pb intercept and Concordia age calculations.

Pb-evaporation results

Zircon crystals from six samples were analyzed by Pb-evaporation: one of enderbite (PMM-09C), two of charnockite (PMM-06 and PMM-20A), one of inequigranular granodiorite (PMM-01), one of leucogranitic vein in pelitic paragneiss (PMM-23A), and one of migmatitic gneiss (PMM-16). Collection locations are shown in Fig. 2, analytical results are presented in Tab. 1, and age *versus* evaporation step diagrams are shown in Fig. 6.

Table 1. Pb-evaporation in zircon isotopic data of rocks from the study area. Common lead correction in accordance with Stacey and Kramers (1975). The evaporation steps used in the mean age calculation are indicated in bold.

Grain number	T (°C)	#ratios	$^{204}Pb/^{206}Pb$	2σ	$^{208}Pb/^{206}Pb$	2σ	$^{207}Pb/^{206}Pb$	2σ	$(^{207}Pb/^{206}Pb)c$	2σ	$(^{207}Pb/^{206}Pb)$ age (Ma)	2σ
PMM-09C – Enderbite												
01	1,450	34	0.000175	5	0.06700	52	0.13190	59	0.12940	51	2090	7
	1,500	36	0.000082	6	0.07679	120	0.13174	21	0.13062	29	2107	4
	1,550	**38**	**0.000125**	**3**	**0.12111**	**49**	**0.13296**	**18**	**0.13129**	**23**	**2116**	**3**
02	1,450	36	0.000187	14	0.04132	37	0.13050	18	0.12807	32	2072	4
	1,500	**32**	**0.000116**	**2**	**0.04884**	**22**	**0.13274**	**38**	**0.13118**	**43**	**2114**	**6**
	1,550	**34**	**0.000133**	**11**	**0.05873**	**44**	**0.13347**	**25**	**0.13164**	**26**	**2120**	**3**
05	1,450	34	0.000229	23	0.06648	164	0.13093	49	0.12798	33	2071	5
	1,500	**34**	**0.000057**	**2**	**0.09307**	**22**	**0.13171**	**16**	**0.13097**	**17**	**2111**	**2**
07	1,450	8	0.001704	448	0.05930	1566	0.13089	85	0.10771	632	1761	107
	1,500	**20**	**0.000136**	**6**	**0.09562**	**56**	**0.13281**	**21**	**0.13117**	**22**	**2114**	**3**
Mean ($^{207}Pb/^{206}Pb$) age (158 isotopic ratios) 2114 ± 3 Ma/USD = 2.24												
PMM-23A – Leucossomatic vein												
01	**1,500**	**40**	**0.000006**	**7**	**0.04573**	**28**	**0.12892**	**31**	**0.12889**	**31**	**2083**	**4**
02	**1,500**	**34**	**0.000006**	**2**	**0.03849**	**18**	**0.12842**	**19**	**0.12837**	**18**	**2076**	**3**
	1,550	**38**	**0.000016**	**4**	**0.03880**	**32**	**0.12830**	**49**	**0.12791**	**42**	**2070**	**6**
03	**1,500**	**36**	**0.000007**	**2**	**0.03604**	**12**	**0.12834**	**18**	**0.12825**	**18**	**2075**	**2**
	1,550	**8**	**0.000017**	**4**	**0.03609**	**50**	**0.12864**	**82**	**0.12842**	**82**	**2077**	**11**
04	**1,500**	**34**	**0.000025**	**4**	**0.03772**	**17**	**0.12847**	**29**	**0.12814**	**30**	**2073**	**4**
05	**1,500**	**28**	**0.000006**	**3**	**0.03879**	**17**	**0.12839**	**24**	**0.12833**	**25**	**2076**	**4**
06	**1,500**	**30**	**0.000015**	**5**	**0.03882**	**15**	**0.12825**	**68**	**0.12807**	**66**	**2072**	**9**
07	**1,500**	**38**	**0.000043**	**19**	**0.03802**	**62**	**0.12848**	**32**	**0.12786**	**48**	**2069**	**7**
	1,550	**4**	**0.000081**	**34**	**0.03838**	**116**	**0.12918**	**38**	**0.12811**	**59**	**2072**	**8**
	1,550	**12**	**0.000071**	**28**	**0.03788**	**122**	**0.12959**	**53**	**0.12777**	**79**	**2068**	**11**
08	**1,450**	**20**	**0.000063**	**6**	**0.04165**	**40**	**0.12915**	**38**	**0.12829**	**39**	**2075**	**5**
	1,500	**38**	**0.000008**	**4**	**0.03831**	**23**	**0.12848**	**33**	**0.12838**	**32**	**2076**	**4**
	1,550	**34**	**0.000000**	**0**	**0.03740**	**14**	**0.12820**	**16**	**0.12820**	**16**	**2074**	**2**
Mean ($^{207}Pb/^{206}Pb$) age (394 isotopic ratios) 2075 ± 2 Ma/USD = 1.46												

Continue...

Table 1 Continuation.

PMM-06 – Charnockite												
03	1,450	28	0.001491	38	0.08927	320	0.14206	28	0.12249	74	1993	11
	1,500	30	0.000093	28	0.18422	324	0.12975	31	0.12774	50	2067	7
	1,550	**36**	**0.000119**	**6**	**0.27484**	**193**	**0.13109**	**21**	**0.12953**	**23**	**2092**	**3**
05	1,450	36	0.000091	4	0.14548	130	0.12855	42	0.12739	57	2063	8
	1,500	**38**	**0.000014**	**2**	**0.25557**	**208**	**0.13000**	**22**	**0.12980**	**21**	**2096**	**3**
06	**1,500**	**32**	**0.000309**	**22**	**0.14642**	**159**	**0.13428**	**30**	**0.13001**	**32**	**2098**	**4**
07	1,450	8	0.000139	24	0.08081	115	0.13072	56	0.12889	64	2083	9
	1,500	**36**	**0.000045**	**4**	**0.09981**	**1081**	**0.12972**	**26**	**0.12919**	**32**	**2087**	**4**
Mean ($^{207}Pb/^{206}Pb$) age (142 isotopic ratios) 2094 ± 4 Ma/USD = 2.32												
Crystal	**T (°C)**	**#ratios**	**$^{204}Pb/^{206}Pb$**	**2σ**	**$^{208}Pb/^{206}Pb$**	**2σ**	**$^{207}Pb/^{206}Pb$**	**2σ**	**($^{207}Pb/^{206}Pb$)c**	**2σ**	**Age (Ma)**	**2σ**
PMM-20A – Charnockite												
01	1,500	40	0.000067	9	0.18159	122	0.13050	34	0.12925	36	2088	5
	1,550	**34**	**0.000010**	**1**	**0.16295**	**83**	**0.12914**	**22**	**0.12912**	**24**	**2086**	**3**
	1,570	**20**	**0.000013**	**14**	**0.12933**	**4**	**0.12924**	**32**	**0.12920**	**32**	**2087**	**4**
03	1,500	16	0.000041	11	0.19330	514	0.12961	53	0.12907	70	2086	10
	1,550	**36**	**0.000041**	**17**	**0.18553**	**148**	**0.12936**	**27**	**0.12888**	**28**	**2083**	**4**
07	1,450	20	0.000136	7	0.14306	202	0.13019	50	0.12845	50	2077	7
	1,500	36	0.000013	5	0.21310	50	0.12845	16	0.12830	18	2075	2
	1,550	**34**	**0.000008**	**1**	**0.17216**	**592**	**0.12901**	**25**	**0.12890**	**25**	**2083**	**3**
08	1,500	38	0.000010	6	0.26223	72	0.12866	31	0.12856	25	2079	3
	1,550	**24**	**0.000006**	**5**	**0.27111**	**351**	**0.12884**	**42**	**0.12880**	**39**	**2082**	**5**
09	**1,450**	**08**	**0.000030**	**14**	**0.26798**	**605**	**0.12924**	**35**	**0.12885**	**40**	**2083**	**5**
	1,500	6	0.000000	0	0.24123	143	0.12955	205	0.12955	205	2092	28
10	**1,550**	**38**	**0.000014**	**4**	**0.16717**	**287**	**0.12892**	**23**	**0.12875**	**23**	**2081**	**3**
11	**1,450**	**24**	**0.000009**	**4**	**0.16378**	**376**	**0.12896**	**48**	**0.12891**	**45**	**2083**	**6**
Mean ($^{207}Pb/^{206}Pb$) age (218 isotopic ratios) 2084 ± 2 Ma/USD = 1.12												
PMM-01 – Inequigranular granodiorite												
02	**1,500**	**22**	**0.000018**	**6**	**0.24519**	**79**	**0.12873**	**45**	**0.12856**	**37**	**2079**	**5**
07	**1,500**	**36**	**0.000016**	**9**	**0.24167**	**92**	**0.12857**	**40**	**0.12845**	**36**	**2077**	**5**
08	**1,500**	**12**	**0.000023**	**2**	**0.26118**	**94**	**0.12893**	**26**	**0.12863**	**28**	**2080**	**4**
09	**1,500**	**8**	**0.000042**	**8**	**0.38122**	**292**	**0.12894**	**68**	**0.12839**	**69**	**2076**	**9**
Mean ($^{207}Pb/^{206}Pb$) age (78 isotopic ratios) 2079 ± 3 Ma/USD = 0.50												
PMM-16 – Migmatitic paragneiss												
01	**1,550**	**38**	**0.000017**	**5**	**0.10241**	**50**	**0.17961**	**36**	**0.17946**	**39**	**2648**	**4**
02	**1,500**	**22**	**0.000372**	**31**	**0.18690**	**342**	**0.13397**	**139**	**0.12892**	**115**	**2084**	**16**
03	**1,500**	**18**	**0.000026**	**2**	**0.03331**	**103**	**0.17505**	**81**	**0.17492**	**102**	**2606**	**10**
	1,550	**6**	**0.000000**	**0**	**0.10128**	**811**	**0.17606**	**117**	**0.17606**	**117**	**2616**	**11**
04	**1,500**	**38**	**0.000013**	**4**	**0.16720**	**54**	**0.12878**	**45**	**0.12869**	**53**	**2080**	**7**
	1,550	**34**	**0.000009**	**6**	**0.14536**	**78**	**0.12845**	**65**	**0.12841**	**69**	**2077**	**9**
05	**1,500**	**20**	**0.000017**	**7**	**0.03636**	**49**	**0.17141**	**52**	**0.17118**	**45**	**2570**	**4**
	1,550	**8**	**0.000000**	**0**	**0.06850**	**272**	**0.17535**	**415**	**0.17535**	**415**	**2610**	**39**
07	**1,500**	**34**	**0.000066**	**7**	**0.04377**	**46**	**0.16976**	**25**	**0.16885**	**31**	**2547**	**3**
08	**1,500**	**34**	**0.000177**	**4**	**0.38958**	**93**	**0.19955**	**36**	**0.19750**	**42**	**2806**	**4**
09	**1,500**	**38**	**0.000277**	**10**	**0.04334**	**44**	**0.16378**	**26**	**0.16019**	**42**	**2458**	**4**
11	**1,550**	**16**	**0.000160**	**5**	**0.60933**	**214**	**0.20594**	**46**	**0.20406**	**42**	**2859**	**3**

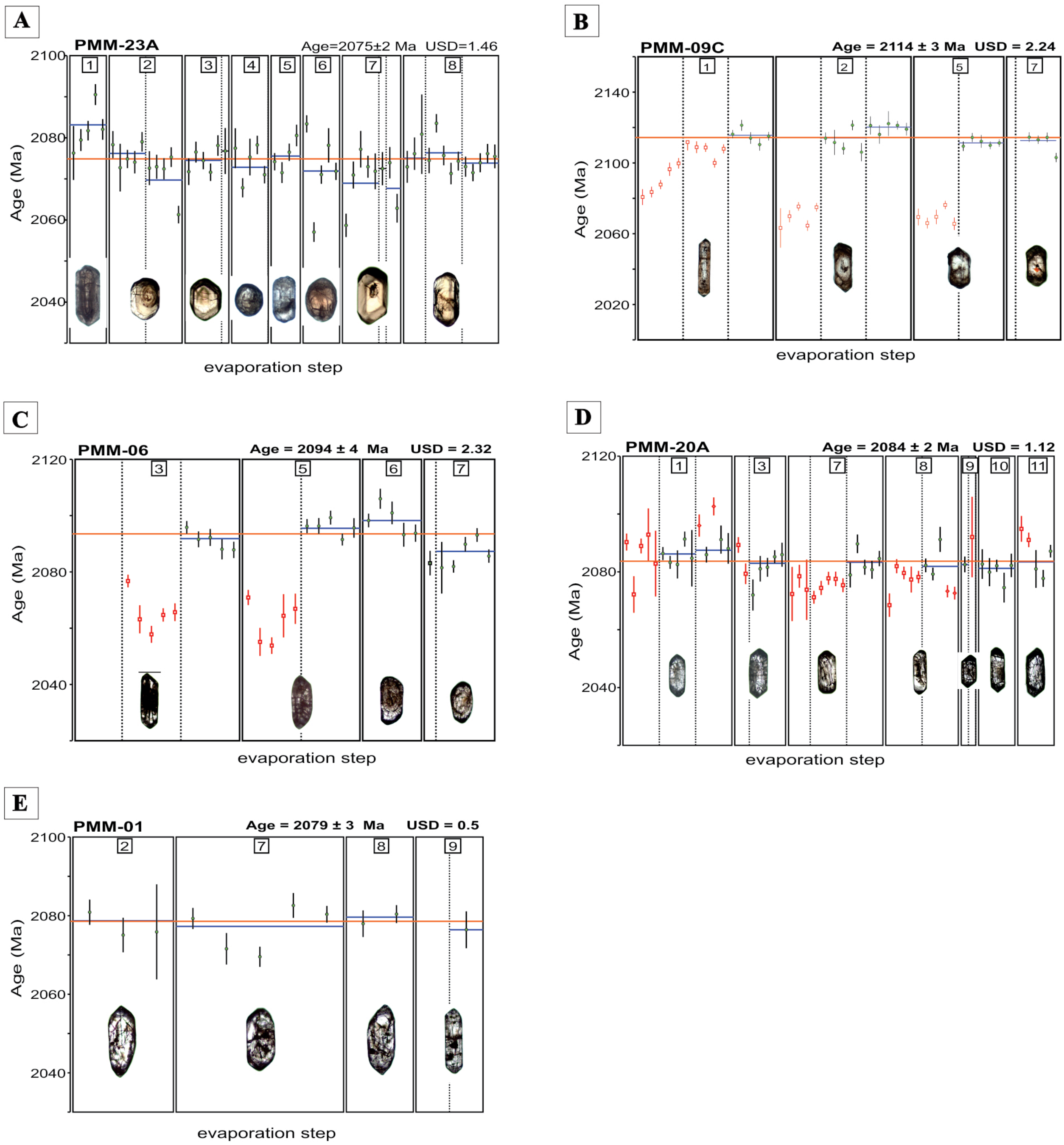

Figure 6. ($^{207}Pb/^{206}Pb$) age *vs.* evaporation steps of zircon crystals. (A) Neosome of paragneiss PMM-23A. (B) Enderbite PMM-09C. (C) Charnockite PMM-06. (D) Charnockite PMM-20A. (E) Granodiorite PMM-01. Isotopic ratio blocks used to calculate the age (green circle); subjectively rejected blocks (red box). USD is $MSWD^{1/2}$.

Leucogranitic vein PMM-23A of pelitic paragneiss

Zircon crystals in sample PMM-23A are generally prismatic, short, bipyramidal, translucent, and brown to caramel in color with rounded edges, suggesting corrosion. Other apparently rounded crystals (Fig. 6A) show small crystalline faces in detail. All eight crystals selected for analysis yielded very reproducible isotopic results that defined an average value of 2075 ± 2 Ma (Tab. 1). This result was interpreted as the crystallization age of the leucogranitic vein (PMM-23A), which, in turn, is the leucosome of pelitic paragneiss (PMM-23B). This is the age of anatexy of pelitic paragneisses from the Middle Xingu River area.

Enderbite PMM-09C

The eight zircon crystals selected from enderbite (sample PMM-09C) for isotopic analysis are euhedral; some are rather elongated or short, bipyramidal, translucent, and brown. The presence of oscillatory zonation in some crystals suggests an igneous origin (Fig. 6B). Very similar isotopic results for four zircon crystals yielded an average age of 2114 ± 3 Ma (Tab. 1) for sample PMM-09C. Even taking the age deviations into account, the calculated ages of the three remainder crystals resulted in a lower age (2087–2098 Ma), possibly due to continuous Pb-loss by metamictization. Therefore, these values were disregarded from the final calculated age. An inherited crystal of 2573 ± 2 Ma was detected in this sample (Tab. 1).

The 2114 ± 3 Ma age obtained for this enderbite is interpreted as the crystallization and emplacement age.

Charnockites PMM-06 and PMM-20A

Nine elongated, bipyramidal, and prismatic zircon crystals — some with smooth edges — were selected from sample PMM-06 for isotopic analysis. The crystals were translucent and brown, with the typical oscillatory zoning of igneous zircon (Fig. 6C). An age of 2094 ± 4 Ma (Tab. 1) was obtained for the sample from four crystals with similar isotopic results. The other crystals presented younger results and, therefore, were disregarded from this calculation.

Eleven euhedral, bipyramidal, elongated, and translucent zircon crystals (some of them were poorly transparent and highly fractured) were selected from sample PMM-20A for isotopic analysis. The crystals are possibly of igneous origin (Fig. 6D). Among the crystals selected for analysis, seven yielded an average age of 2084 ± 2 Ma (Tab. 1). Regarding the remainder crystals, two yielded lower ages and were disregarded from the final calculation, while the other two indicated an inheritage of 2436 ± 33 Ma and 2108 ± 5 Ma (Tab. 1). The last age is correlated to the enderbite bodies. The ages of 2094 ± 4 Ma and 2084 ± 2 Ma are interpreted as crystallization and emplacement ages for these charnockites.

Granodiorite PMM-01

The nine zircon crystals selected from the inequigranular granodiorite sample (PMM-01) for analysis are mostly prismatic and elongated with bipyramidal shapes and bulging edges. Some are translucent while others are transparent and intensely fractured (Fig. 6E). Four of the selected crystals provided reproducible results that defined an average age of 2079 ± 3 Ma (Tab. 1) for the sample, which was interpreted as the age of crystallization, i.e., the emplacement of the granodiorite body. Two inherited crystals of Archean ages of 2824 ± 22 Ma and 2613 ± 8 Ma, and three other crystals of Paleoproterozoic ages of 2415 ± 10 Ma, 2157 ± 3 Ma, and 2107 ± 18 Ma were also detected in this granodiorite. Some of these inherited grains can be from porphyroclastic monzogranite (sample MVD-115) and orthogneisses – the host rocks (Fig. 2).

Migmatitic gneiss PMM-16

Twelve zircon crystals of leucosome of migmatitic gneiss were selected, sample PMM-16. These crystals show long or short bipyramidal and slightly rounded shapes. Some grains were translucent, while a few crystals were transparent, and other grains showed intense metamictization. Ages from 2077 ± 9 Ma to 2859 ± 3 Ma (Tab. 1) were obtained for this leucosome, which is unsuitable for calculating a satisfactory mean age but covers the range of values available for the study area — including crystallization ages of inherited crystals. In contrast, three distinct age groups could be calculated, one of approximately 2.86 Ga (two crystals), an intermediate one of 2.65–2.36 Ga (eight crystals), and a lower one of 2.08 Ga (two crystals). This last age can be interpreted as the minimum crystallization age of the leucosome of migmatitic gneiss. The older grains correspond to the inherited zircon crystals of the protolith of this migmatitic gneiss whose large range of Archean to Siderian (minimum) ages can suggest a paraderived source. The anatectic age of this gneiss was contemporary with the charnockites and the granodiorite.

U-Pb SHRIMP results

Crystals from two zircon samples of tonalitic orthogneisses (PMM-4B and PMM-02A) and a sample of monazite of pelitic paragneiss (PMM-23B) were dated through the U-Pb SHRIMP method. This *in situ* analysis allows dating of metamorphic overgrowth in zircon and monazite crystals. CL and BSE images were applied to select overgrowths, patchy, and sector zones for dating (Fig. 7). Analytical results are presented in Tabs. 2–4, while calculated ages in Concordia diagrams are shown in Fig. 8.

Tonalitic orthogneiss PMM-04B

The zircon crystals of sample PMM-04B are euhedral to subhedral, elongated, bipyramidal, brown, rarely translucent, semi-translucent, or opaque. Some crystals show igneous oscillatory zoning (Fig. 7A) and inclusions, but most zircon grains have patchy zoning, alteration pathways, and metamitic zones (Fig. 7B). These last features are related to late alteration, but patchy zoning suggests recrystallization by high-grade metamorphism (Corfu *et al.* 2003). Most points are significantly discordant, but some ages were calculated (Fig. 8A and Tab. 2):

- An age defined by the weighted mean $^{207}Pb/^{206}Pb$ values from the five most concordant analyses yields 2480 ± 9 Ma.

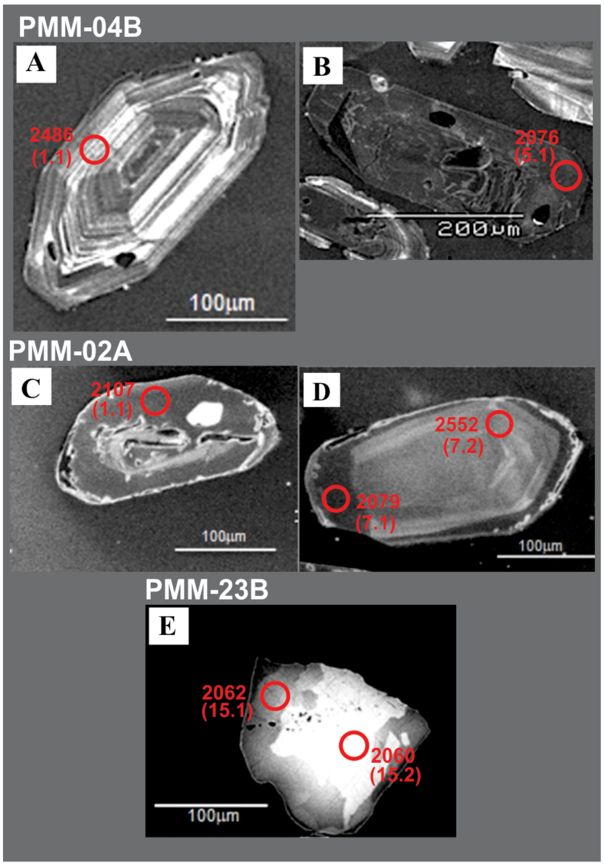

Figure 7. Cathodoluminescence images of zircon crystals of the samples (A and B) PMM-04B and (C and D) PMM-02A, with igneous oscillatory and patchy zoning, microfractures, alteration pathways, and metamitic zones. Backscattered electron image of a monazite crystal of sample PMM-23B with (E) convolute zoning. Crystals showing their respective SHRIMP spots (spot number) and $^{207}Pb/^{206}Pb$ ages in Ma.

Table 2. Summary of SHRIMP U-Pb zircon data for sample PMM-04B[#,$].

Grain Spot	$^{206}Pb_c$ (%)	U (ppm)	Th (ppm)	$^{232}Th/^{238}U$	$^{206}Pb^*$ (ppm)	(1) $^{206}Pb/^{238}U$ Age		(1) $^{207}Pb/^{206}Pb$ Age		Discordant (%)	(1) $^{207}Pb^*/^{206}Pb^*$	± %	(1) $^{207}Pb^*/^{235}U$	± %	(1) $^{206}Pb^*/^{238}U$	± %	Errors correlation
1.1	0.08	14	11	0.81	4.78	2215	± 27	2486	± 13	11	0.1629	0.76	9.21	1.6	0.4101	1.4	0.884
2.1	7.19	34	19	0.59	6.17	1151	± 15	2351	± 46	51	0.1505	2.7	4.06	3	0.1955	1.4	0.454
2.2	2.02	54	13	0.25	17	1967	± 19	2434	± 15	19	0.158	0.88	7.77	1.4	0.3568	1.1	0.792
3.1	0.65	20	9	0.47	8.09	2510	± 28	2478	± 16	-1	0.1622	0.96	10.64	1.7	0.476	1.4	0.818
4.1	0.05	47	37	0.81	16.1	2159	± 21	2467	± 7.1	12	0.16109	0.42	8.83	1.2	0.3977	1.1	0.938
5.1	1.64	103	29	0.29	32.5	1982	± 18	2076	± 19	5	0.1284	1.1	6.372	1.5	0.3599	1.1	0.714
6.1	0.34	135	59	0.45	38.3	1835	± 17	2414	± 9.2	24	0.15611	0.54	7.089	1.2	0.3293	1.1	0.889
7.1	0.03	221	124	0.58	58.9	1740	± 16	2387	± 3.7	27	0.15369	0.22	6.568	1.1	0.3099	1	0.978
8.1	0.27	68	20	0.30	17.8	1706	± 18	2415	± 12	29	0.1562	0.7	6.526	1.4	0.303	1.2	0.860
9.1	0.11	95	23	0.25	32.6	2158	± 20	2482	± 5	13	0.16251	0.3	8.909	1.1	0.3976	1.1	0.963
10.1	0.76	42	18	0.44	16.7	2417	± 23	2482	± 22	3	0.1625	1.3	10.19	1.8	0.4549	1.1	0.652
11.1	–	18	9	0.50	7.05	2403	± 26	2478	± 10	3	0.16212	0.6	10.1	1.4	0.4518	1.3	0.909
12.1	–	76	46	0.63	32	2578	± 23	2481	± 5.3	-4	0.16238	0.32	11.01	1.1	0.4916	1.1	0.960
13.1	1.28	37	15	0.43	7.13	1300	± 14	2433	± 17	47	0.1579	1	4.862	1.6	0.2234	1.2	0.763
14.1	0.18	140	16	0.12	51.8	2297	± 22	2546	± 4.4	10	0.16882	0.26	9.97	1.2	0.4281	1.1	0.974
15.1	1.51	21	14	0.68	6.74	2015	± 22	2479	± 19	19	0.1622	1.1	8.21	1.7	0.3669	1.3	0.748
16.1	0.36	134	58	0.45	43.4	2055	± 21	2494	± 5	18	0.16369	0.3	8.48	1.2	0.3755	1.2	0.970
17.1	3.32	22	8	0.37	9.24	2506	± 27	2483	± 23	-1	0.1626	1.4	10.66	1.9	0.4751	1.3	0.686
18.1	0.09	134	31	0.24	41.6	1984	± 18	2073	± 6.2	4	0.12815	0.35	6.369	1.1	0.3604	1.1	0.950

[#]Errors are 1-sigma; Pb_c and Pb*: the common and radiogenic portions, respectively; [$]error in standard calibration was 0.18% (not included in above errors but required when comparing data from different mounts); (1) common Pb corrected using measured ^{204}Pb.

Table 3. Summary of SHRIMP U-Pb zircon data for sample PMM-02A[#,$].

Grain Spot	$^{206}Pb_c$ (%)	U (ppm)	Th (ppm)	$^{232}Th/^{238}U$	$^{206}Pb^*$ (ppm)	(1) $^{206}Pb/^{238}U$ Age		(1) $^{207}Pb/^{206}Pb$ Age		Discordant (%)	(1) $^{207}Pb^*/^{206}Pb^*$	± %	(1) $^{207}Pb^*/^{235}U$	± %	(1) $^{206}Pb^*/^{238}U$	± %	Errors correlation
1.1	–	274	14	0.05	91	2107	± 18	2107	± 4.1	0	0.13065	0.23	6.965	1	0.3867	1	0.974
2.1	0.29	61	36	0.61	22	2263	± 20	2541	± 6.9	11	0.16833	0.41	9.76	1.1	0.4205	1.1	0.931
3.1	–	659	33	0.05	144	1463	± 14	2173	± 10	33	0.1357	0.6	4.768	1.3	0.2548	1.1	0.879
3.2	–	52	31	0.60	14.5	1800	± 19	2541	± 13	29	0.1684	0.75	7.48	1.4	0.3221	1.2	0.847
4.1	0.11	29	20	0.72	11.7	2492	± 23	2517	± 7.4	1	0.16591	0.44	10.79	1.2	0.4718	1.1	0.928
5.1	0.88	410	22	0.06	29.1	507	± 5.6	1122	± 21	55	0.07704	1	0.869	1.5	0.08185	1.2	0.745
6.1	–	222	27	0.12	87.3	2429	± 21	2553	± 3.5	5	0.16956	0.21	10.7	1	0.4575	1	0.979
7.1	–	287	18	0.07	91.9	2044	± 18	2079	± 2.9	2	0.12859	0.17	6.617	1	0.3732	1	0.987
7.2	–	148	162	1.13	60.6	2510	± 21	2552	± 3.2	2	0.16947	0.19	11.12	1	0.476	1	0.983
8.1	0.59	26	13	0.50	10.3	2407	± 23	2449	± 12	2	0.1594	0.71	9.95	1.3	0.4527	1.1	0.845
9.1	0.15	93	33	0.36	33.9	2269	± 20	2538	± 5.7	11	0.16803	0.34	9.77	1.1	0.4218	1	0.950
10.1	0.15	48	29	0.62	18.1	2355	± 21	2520	± 7.1	7	0.16625	0.42	10.11	1.1	0.441	1.1	0.930
11.1	–	192	64	0.34	74.8	2410	± 21	2502	± 7.8	4	0.16441	0.47	10.27	1.1	0.4532	1	0.910
12.1	–	210	102	0.50	86.3	2521	± 21	2555	± 2.8	1	0.16976	0.17	11.2	1	0.4786	1	0.987
13.1	–	412	96	0.24	152	2296	± 19	2410	± 4.8	5	0.15573	0.28	9.188	1	0.4279	1	0.963
15.1	0.01	398	62	0.16	78.7	1335	± 12	2336	± 14	43	0.1491	0.8	4.731	1.3	0.2301	1	0.785
16.1	2.13	183	26	0.15	44.3	1575	± 15	2022	± 17	22	0.1245	0.99	4.752	1.4	0.2767	1	0.726
17.1	0.00	385	63	0.17	158	2519	± 21	2540	± 2.2	1	0.16818	0.13	11.09	1	0.4782	1	0.992
18.1	–	362	17	0.05	119	2088	± 18	2108	± 3	1	0.13075	0.17	6.894	1	0.3824	1	0.987
19.1	0.41	110	47	0.44	44.3	2459	± 22	2543	± 5.1	3	0.16851	0.31	10.79	1.1	0.4645	1.1	0.963
20.1	0.12	50	34	0.70	19.6	2438	± 22	2557	± 6.5	5	0.16996	0.39	10.77	1.1	0.4596	1.1	0.940
21.1	–	166	8	0.05	64.3	2405	± 21	2507	± 3.4	4	0.16496	0.2	10.28	1	0.4522	1	0.981
22.1	–	187	21	0.11	65.2	2200	± 19	2255	± 7	2	0.14227	0.41	7.979	1.1	0.4067	1	0.930

[#]Errors are 1-sigma; Pb_c and Pb^*: the common and radiogenic portions, respectively; [$]error in standard calibration was 0.18% (not included in above errors but required when comparing data from different mounts); (1) Common Pb corrected using measured ^{204}Pb.

Table 4. Summary of SHRIMP U-Pb monazite data for sample PMM-23B[#,$].

Grain Spot	$^{206}Pb_c$ (%)	U (ppm)	Th (ppm)	$^{232}Th/^{238}U$	$^{206}Pb^*$ (ppm)	(1) $^{206}Pb/^{238}U$ Age		(1) $^{207}Pb/^{206}Pb$ Age		Discordant (%)	(1) $^{207}Pb^*/^{206}Pb^*$	± %	(1) $^{207}Pb^*/^{235}U$	± %	(1) $^{206}Pb^*/^{238}U$	± %	Errors correlation
1.1	0.09	2,734	51,588	19.5	891	2072	±23	2059	±5.5	-1	0.12715	0.31	6.645	1.3	0.379	1.3	0.973
2.1	0.07	2,011	46,813	24.1	639	2027	±23	2069.9	±6.4	2	0.12794	0.36	6.518	1.4	0.3695	1.3	0.965
3.1	0.01	2,229	41,559	19.3	705	2021	±23	2058.7	±6.6	2	0.12713	0.37	6.454	1.4	0.3682	1.3	0.963
3.2	0.01	7,442	54,844	7.6	2410	2062	±23	2086.8	±4.3	1	0.12918	0.24	6.713	1.3	0.3769	1.3	0.982
4.1	0.02	2,553	42,837	17.3	800	2005	±23	2065	±5.4	3	0.12759	0.3	6.418	1.4	0.3648	1.3	0.974
5.1	0.05	2,563	41,759	16.8	833	2067	±23	2059.1	±5.6	0	0.12716	0.32	6.63	1.4	0.3781	1.3	0.972
5.2	0.05	1,242	63,033	52.5	402	2062	±24	2057.4	±7.4	0	0.12704	0.42	6.604	1.4	0.377	1.4	0.957
6.1	1.70	927	56,016	62.4	299	2023	±33	2068	±47	2	0.1278	2.7	6.5	3.3	0.3686	1.9	0.576
6.2	0.10	385	66,854	179.5	121	2004	±28	2056	±14	3	0.127	0.81	6.38	1.8	0.3647	1.6	0.893
7.2	0.01	1,945	53,535	28.4	624	2045	±24	2064.6	±6.2	1	0.12756	0.35	6.565	1.4	0.3733	1.4	0.969
8.1	0.05	1,795	35,017	20.2	576	2044	±24	2058.1	±6.4	1	0.12709	0.36	6.538	1.4	0.3731	1.4	0.966
9.1	0.05	2,226	62,599	29.1	716	2049	±24	2061	±6	1	0.1273	0.34	6.566	1.4	0.3741	1.4	0.970
10.1	0.02	2,270	42,196	19.2	741	2075	±24	2056.1	±5.7	-1	0.12695	0.32	6.646	1.4	0.3797	1.4	0.973
11.1	0.00	1,868	52,216	28.9	598	2043	±24	2060.1	±6.3	1	0.12723	0.36	6.54	1.4	0.3728	1.4	0.968
12.1	0.04	404	69,842	178.5	135	2118	±30	2083	±13	-2	0.12893	0.76	6.92	1.8	0.389	1.6	0.908
13.1	0.06	406	64,703	164.8	132	2075	±30	2069	±13	0	0.12787	0.72	6.7	1.9	0.3797	1.7	0.921
14.1	0.00	1,561	68,054	45.0	504	2056	±24	2068.8	±6.6	1	0.12786	0.37	6.622	1.4	0.3756	1.4	0.965
15.1	0.00	2,333	41,203	18.3	750	2048	±24	2061.9	±5.7	1	0.12736	0.32	6.568	1.4	0.374	1.4	0.973
15.2	0.11	444	64,647	150.3	143	2053	±28	2060	±13	0	0.12724	0.75	6.58	1.8	0.375	1.6	0.906
16.1	0.01	3,769	30,824	8.5	1210	2042	±23	2056.4	±4.8	1	0.12697	0.27	6.525	1.4	0.3728	1.3	0.980

[#]Errors are 1-sigma; Pb_c and Pb*: the common and radiogenic portions, respectively; [$]error in standard calibration was 0.18% (not included in above errors but required when comparing data from different mounts); (1) common Pb corrected using measured ^{204}Pb.

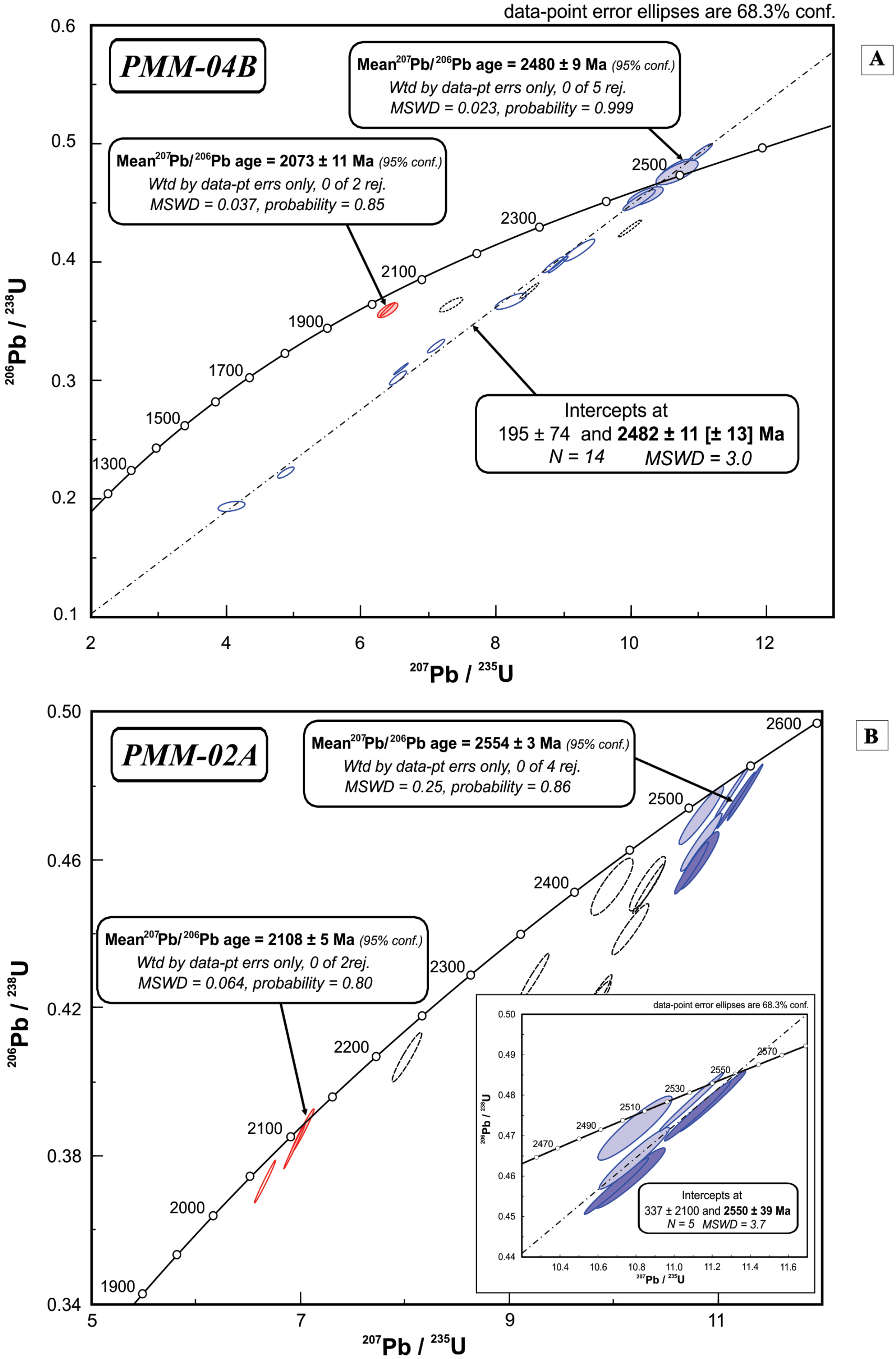

Figure 8. Concordia diagrams with analytical points of zircon crystals of the samples (A) PMM-04B and (B) PMM-02A. The dashed ellipses are results not included in calculations.

The discordant data follow a trend but with significant scattering. Regression of the data concerning this generation resulted in an upper intercept age of 2482 ± 11 Ma with an MSWD of 3.0;

- A weighted mean $^{207}Pb/^{206}Pb$ age of 2073 ± 11 Ma (95% confidence limits on two data points: 5.1 and 18.1; see Tab. 2).

The age of 2480 ± 9 Ma is interpreted as the crystallization age of the igneous protolith (tonalite) of this orthogneiss, whereas the other one (2073 ± 11 Ma) dates the high-grade metamorphic event that affected this tonalite.

Tonalitic orthogneiss PMM-02A

The zircon crystals of orthogneiss PMM-02A are subhedral to euhedral, sometimes presenting rounded edges. In general, zircon grains are semi-translucent to opaque, brown, and rather fractured crystals containing few inclusions. Most of the crystals have patchy overgrowth rims and sector zoning (Fig. 7C) with blurred igneous oscillatory zoning (Fig. 7D). These features suggest a strong high-grade metamorphic recrystallization of zircon crystals. Microfractures, alteration pathways, and metamitic zones are also present in these zircon grains. Due to the complexity and poor preservation of the igneous zircon crystals, it was difficult to calculate an age for the protolith, but seven crystals furnish an upper intercept age at 2550 ± 39 Ma (MSWD = 3.7). Otherwise, four selected crystals yielded a mean $^{207}Pb/^{206}Pb$ age of 2554 ± 3 Ma (MSWD = 0.25), which can represent the minimum crystallization age for this sample. Scattering is clearly present, probably due to early Pb-loss. Two analyses (1.1 and 18.1; Tab. 3) are concordant and give a mean weighted $^{207}Pb/^{206}Pb$ age of 2108 ± 5 Ma, and just one subconcordant grain (7.1; Tab. 3) yields a $^{207}Pb/^{206}Pb$ age of 2079 ± 3 Ma (Figs. 7C and 7C, and 8B).

Pelitic paragneiss PMM-23B

The monazite crystals of the pelitic paragneiss PMM-23B are anhedral to subhedral and usually fragmented and fractured. BSE images reveal rim-and-core structures with convoluted zoning (Fig. 7E). SHRIMP U-Pb analyses of 13 concordant or near-concordant (maximum 2% discordance, see Tab. 4) spots give a Concordia age of 2062 ± 8 Ma with an MSWD = 1.16 (Fig. 9).

DISCUSSION

Late Rhyacian collisional orogeny

The Paleoproterozoic collision between Africa and South America plates was recognized by Ledru *et al.* (1994), which showed lithological associations and tectonic structures related to the Transamazonian orogeny in the northern Guiana shield. Delor *et al.* (2003) distinguished an oblique convergence between these continental blocks marked by sinistral sliding shear zones (blockage), emplacement of granites, local formation of pull-apart basin, and migmatites between 2.10 and 2.08 Ga. This stage was followed by crustal stretching with continental-scale boudins in granulite belts (Imataca, Bakhuis, and Amapá block) with local ultra-high-temperature (UHT) metamorphism and the emplacement of charnockites between 2.07 and 2.05 Ga (Delor *et al.* 2003, De Roever *et al.* 2003). These previous models supported the proposal of syn-collisional (2.11–2.09 Ga) and post-collisional (2.08–2.06 Ga) stages of the Transamazonian cycle in the southern part of MIP (Vasquez *et al.* 2008b, 2014). However, the post-collisional stage can be extended up to 2.03 Ga (Rosa-Costa *et al.* 2008, 2009).

Geochronological results

In the study area, the high-grade metamorphic rocks are orthogneiss and paragneiss that underwent anatexy — as testified by their migmatitic structures. The aluminous minerals assemblages indicate pelitic protoliths to the paragneisses, and the orthogneisses predominantly are of tonalitic protoliths. Gneisses and granofels presenting two pyroxenes were not found, but a granulite mineral assemblage was identified in previous geological mapping with granulites and retrogranulites in areas around the study area (Vasquez *et al.* 2008b, 2008c, 2014). Microtextures of both types of gneiss indicated that the high-temperature (> 550°C) recrystallization fabric of these rocks was overprinted by low-temperature (< 550°C) recrystallization bands, probably during retrograded metamorphism. The U-Pb SHRIMP dating of the zircons from these orthogneisses (samples PMM-02A and PMM-04B) yielded crystallization ages of around 2.5 Ga for tonalite protoliths and ages of metamorphic events of 2.11 and 2.07 Ga (Tab. 5). Both results are coherent with the Bacajá domain crustal evolution due to dating (through the same method) of a tonalitic gneiss of ca. 2.5 Ga in the western portion of this domain (Santos 2003, Vasquez *et al.* 2008a). The Late Rhyacian ages of 2.11 and 2.07 Ga may be related to high-grade metamorphic events of collisional orogeny during the Transamazonian cycle, as previously proposed (Macambira *et al.* 2007, Vasquez *et al.* 2008b, 2014). In our results, there is an age gap from 2108 ± 5 Ma (sample PMM-02A) to 2073 ± 11 Ma (sample PMM-04B) suggesting different stages of continental collision.

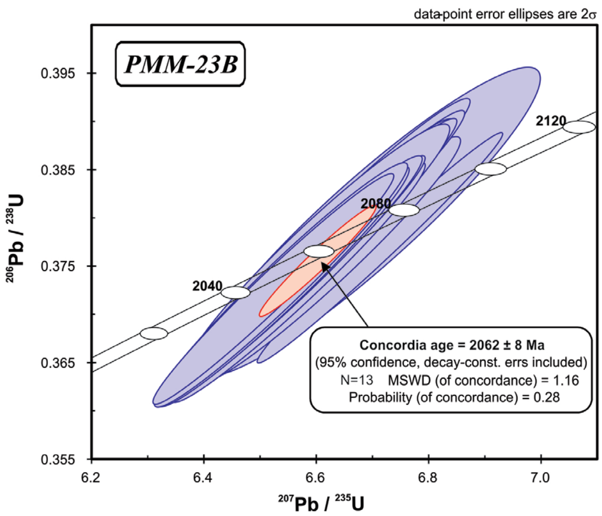

Figure 9. Concordia diagram with analytical points of monazite crystals of the sample PMM-23B.

A leucogranitic vein, that is a leucosome of a pelitic paragneiss (sample PMM-23B), resulted in a Pb-evaporation age of 2075 ± 2 Ma, that is, the anatectic age of this rock, whereas the monazite hosted by pelitic paragneiss (sample PMM-23B) yielded a U-Pb SHRIMP age of 2062 ± 8 Ma (Tab. 5). Both ages are similar and related to high-grade metamorphism.

A strongly migmatized gneiss (sample PMM-16), in the southern portion of the Middle Xingu River area, resulted in a Pb-evaporation age of 2080 ± 5 Ma for its leucosome crystallization. This migmatitic gneiss has inherited zircon crystals of 2.86–2.35 Ga with grains of 2.65 and 2.46 Ga, which indicate sources from Neoarchean and Siderian protoliths from the Bacajá domain and/or a minimum age for these grains.

The charnockitic and granitic rocks, which cut gneisses and retrogranulites, predominate in the study area. Two pyroxenes relics, i.e., mesopertite and antipertite, distinguished the charnockitic rocks from the other granitic rocks. These rocks usually have porphyroclastic and granoblastic textures as well as low-temperature recrystallization bands and preserved igneous textures. Microtextures of ductile deformation are more frequent in enderbites than in charnockites bodies; these ones cut the first ones. The enderbite (sample PMM-09C) yielded a zircon Pb-evaporation age of 2114 ± 3 Ma, while the two charnockites resulted in ages of 2094 ± 4 Ma (sample PMM-20A) and 2084 ± 2 Ma (sample PMM-06). These results support that enderbites are older than charnockites and distinguish two generations of charnockitic rocks. The 2.11–2.09 Ga charnockites are related to a syn-collisional stage and the ca. 2.08 Ga charnockites are related to a post-collisional stage (Vasquez *et al.* 2008b).

Two groups of granitic rocks outcrop in the study area: a small intrusion of porphyroclastic monzogranite of 2.15 Ga (sample MVD-115: Vasquez *et al.* 2008a) and batoliths. Placed between the batoliths, a granodiorite (sample PMM-01) with preserved igneous texture yielded a zircon Pb-evaporation age of 2079 ± 3 Ma and presented inherited zircon grains of 2.82–2.16 Ga (Tab. 5). The monzogranite of 2.15 Ga is probably related to the pre-collisional stage of the Bacajá domain (Vasquez *et al.* 2008a), while the granodiorite of 2.08 Ga is related to the post-collisional stage.

Correlations and geochronological province limits

Late Rhyacian (2.10–2.07 Ga) zircon ages were obtained for granitic and charnockitic rocks from the north of the Bacajá domain (Santos 2003, Faraco *et al.* 2005, Vasquez *et al.* 2005, 2008a, Macambira *et al.* 2009). Ages for metamorphic rocks of 2.09 and 2.07 Ga were obtained by applying the U-Pb SHRIMP to zircon crystals, respectively, in a paragneiss and an orthogneiss from the southeastern portion of the Bacajá domain. The monazite of this paragneiss yielded an age of 2.06 Ga (Macambira *et al.* 2007). Zircon and monazite crystals of paragneisses from northwest of the domain yielded metamorphic ages of 2.13–2.11 Ga and 2.07–2.06 Ga (Vasquez *et al.* 2014). These previous geochronological data constrained the high-grade metamorphism of igneous and sedimentary rocks from Bacajá domain to late Rhyacian, which correspond to the time of emplacement of granitic and charnorckitic rocks related to the syn- and post-collisional stages of the Transamazonian orogenic cycle (Vasquez *et al.* 2008a, 2008b, 2014, Macambira *et al.* 2007, 2009). Similarly, the late Rhyacian ages obtained in this study for rocks from the southeastern Bacajá domain (Middle Xingu River area) are also related to this stage of collisional orogeny (Tab. 5).

In the northern part of MIP (Guiana shield), Rosa-Costa *et al.* (2008) dated the high-grade metamorphism around 2.09 and 2.05 Ga by U-Th-Pb in monazite from migmatites, granulites, and orthogneisses of the Amapá block (Fig. 1B). Granitic rocks were emplaced between 2.05 and 2.03 Ga in this high-grade metamorphic belt (Rosa-Costa *et al.* 2006). UHT metamorphism was identified by De Roever *et al.* (2003) in granulites from the Bakhuis belt in the central part of the shield (Fig. 1B). Zircon ages of 2.07–2.05 Ga that these authors obtained for high-grade metamorphism using the Pb-evaporation method were like the age of about 2.06 Ga of charnockitic bodies and associated mafic intrusions. This high-grade metamorphism of 2.07–2.05 Ga was also identified in the Imataca block (Tassinari *et al.* 2004), in the northwestern part of the shield (Fig. 1B). Late Rhyacian magmatism and high-grade metamorphism occur throughout the MIP and

Table 5. Summary of geochronological data of rocks from Middle Xingu River area.

Rock type/sample	Magmatic age (Ma)	Inherited age (Ma)	Metamorphic age (Ma)	Method/mineral
Tonalitic orthogneiss/PMM-02A	2554 ± 3		2108 ± 5	S/zr
Tonalitic orthogneiss/PMM-04B	2480 ± 9		2073 ± 11	S/zr
Monzogranite/MVD115B	2147 ± 5*			S/zr
Enderbite/PMM-09C	2114 ± 3	2573 ± 2		E/zr
Charnockite/PMM-06	2094 ± 4			E/zr
Charnockite/PMM-20A	2084 ± 2	2108 ± 5;2436 ± 33		E/zr
Migmatitic gneiss/PMM-16	2080 ± 5	2364 ± 9;2458 ± 6; 2648 ± 4;2859 ± 3		E/zr
Granodiorite/PMM-01	2079 ± 3	2157 ± 3;2415 ± 10; 2613 ± 8;2824 ± 22		E/zr
Leucogranitic vein/PMM-23A	2075 ± 2			E/zr
Pelitic paragneiss/PMM-23B			2062 ± 8	S/mnz

S: U-Pb SHRIMP; E: Pb-evaporation; zr: zircon; mnz: monazite; *Vasquez *et al.* (2008a).

are important geological records for the delimitation of this geochronological province and the Transamazonian cycle.

Neoarchean and Siderian rocks are present in the Bacajá domain. In the central portion of this domain, a 2.7 Ga juvenile orthogneiss (Macambira *et al.* 2009) outcrops. In the northwestern and northeastern portions of this domain, orthogneisses of 2.5–2.44 Ga (Santos 2003, Vasquez *et al.* 2005, Macambira *et al.* 2009) outcrop. Metandesites and metadacites of 2.45–2.36 Ga with crustal-source magma of about 2.6 Ga (Vasquez *et al.* 2008a, Macambira *et al.* 2009) are also present in this domain. Mesoarchean rocks locally occur in the Bacajá domain. The orthogranulites from the southeastern and eastern parts of this domain not only have a source of 3.0–2.94 Ga, but also a source of ca. 2.6 Ga (Macambira *et al.* 2007, Vasquez *et al.* 2008b). Rosa-Costa *et al.* (2006) identified only the traces of Mesoarchean crust (inherited zircon grains and Nd-model ages) associated with orthogranulites and orthogneisses with protoliths of 2.78–2.63 Ga from the Amapá block. However, these evidences of the Archean crust are rare in both the Bakhuis belt (De Roever *et al.* 2015) and the Cauarane-Coeroeni belt in the Central Guiana shield (Nadeau *et al.* 2013). The occurrence of reworked Archean crust during the Paleoproterozoic is greater in the southeastern MIP (Bacajá domain), probably due to its proximity to the Archean crust of the CAP.

The presence of juvenile magmas of around 2.6 Ga and the formation of rocks from 2.67 to 2.44 Ga are key features to distinguish the CAP and MIP, because, in the Carajás block, the youngest Neoarchean granites are of about 2.57 Ga (Old Salobo granites) (Machado *et al.* 1991, Melo *et al.* 2016, Toledo *et al.* 2019). The other granites, gneisses, metavulcano-sedimentary rocks, diorites, gabbros, and ultramafic rocks of the Carajás block were formed between 3.00 and 2.73 Ga with an Nd-T_{DM} of about 3.0 Ga (zircon geochronology and Nd-isotopic data, respectively, are compiled in table 2.2 of Vasquez *et al.* 2008b).

Mesoarchean rocks predominate in the central and southern parts of the Carajás block, whereas the Neoarchean rocks are restricted to the northern part whose basement is composed of Mesoarchean rocks. The Mesoarchean protolith (3.0 Ga) of an orthogneiss (retrogranulite) with a metamorphic age of 2.07 Ga (Macambira *et al.* 2007) in the southeastern of the Bacajá domain suggests that this orthogneiss could represent a part of the Carajás block that was tectonically dismembered by the Transamazonian cycle.

The CAP-MIP boundary is also marked by an E-W system fault that controls a supracrustal belt of ca. 2.76 Ga (Grão Pará, Igarapé Salobo, and other correlated groups) from the Carajás block. In the eastern part of this boundary, thrust faults have imbricated rocks of Bacajá domain over Archean rocks of Carajás blocks during the compressive event D2 (Bacajá-Carajás collision) that had tectonically transported them to the SW direction between 2.10 and 2.06 Ga (Tavares *et al.* 2018). However, nappes of Rhyacian rocks from the Bacajá domain have not been identified yet, only sedimentary rocks (Águas Claras Formation), probably deposited during D2, were preserved. Rb-Sr and K-Ar ages of ca. 2.0 Ga presented by Cordani *et al.* (1984) for the supracrustal rocks of this region suggest that the event D2 reached at least greenschist conditions of metamorphism.

In the western CAP-MIP boundary, the E-W system fault is bordering the supracrustal rocks of 2.76 Ga from the Carajás block. In this area, the migmatitic gneiss (Fig. 2), which has inherited zircon crystals of 2.86–2.36 Ga and furnished a crystallization age of 2.07 Ga for the leucosome of sample PMM-16 (Tab. 5), supports that this high-grade rock is from the Bacajá domain. This migmatitic gneiss is the Rhyacian rock closest to the CAP-MIP boundary.

CONCLUDING REMARKS

Field data and petrographic studies of rocks from the Middle Xingu River area, supporting the zircon and monazite Pb-evaporation and U-Pb SHRIMP data, allowed the following remarks.

The protoliths of tonalitic orthogneiss, crystallized at ca. 2.5 Ga, are present in other parts of the Bacajá domain (southern MIP) but are rare in the Carajás block (eastern PAC). These orthogneisses were reworked at around 2.11 and 2.07 Ga, the ages at which high-grade metamorphism occurred in the Bacajá domain. The pelitic paragneisses of the Bacajá domain also underwent this high-grade metamorphism in the late Rhyacian, as shown by their leucosome veins of 2.07 Ga and the monazite crystals of 2.06 Ga from hosted pelitic paragneiss.

Two generations of charnockitic rocks were distinguished with enderbites of 2.11 Ga and charnockites of ca. 2.08 Ga. These ages agreed with the high-grade metamorphism that occurred in the late Rhyacian, which is correlated to the Bacajá-Carajás collision, between 2.1 and 2.06 Ga.

The gap between the high-grade metamorphism and the magmatism suggested that the ca. 2.1 Ga event was related to a syn-collisional stage, and the ca. 2.07 Ga stage was related to a post-collisional stage of the Transamazonian orogenic cycle.

Granitic rocks of 2.08 Ga were also emplaced during the post-collisional stage, and pre-collisional granites of ca. 2.15 Ga locally outcrop in the southwestern portion of the Bacajá domain.

Located in the southern portion of the Middle Xingu River area, the migmatitic gneiss with a leucosome of 2.08 Ga is the rock, reworked during the Rhyacian, closest to the Carajás block. Therefore, this rock marks the western MIP-CAP boundary.

ACKNOWLEDGMENTS

The authors acknowledge the Brazilian National Council for Scientific and Technological Development (CNPq) for the research fellowship granted to the first author and the master's fellowship granted to the third author as part of his Postgraduate Program in Geology and Geochemistry at the Universidade Federal do Para (UFPA). Acknowledgments are also extended to the Geological Survey of Brazil (CPRM) and the CT-Mineral/FINEP 01/2001 Project, for fieldwork funding, and the Isotopic Geology Laboratory (Para-Iso) at UFPA. The authors dedicate a special acknowledgment to Dr. M.A. Galarza for his helpful support in spectrometric analyses.

ARTICLE INFORMATION
Manuscript ID: 20220017. Received on: 29 JAN 2022. Approved on: 28 JUN 2022.

How to cite this article: Macambira M.J.B., Vasquez M.L., Monteiro P.C., Armstrong R.A. Archean to Rhyacian crustal records along the Middle Xingu River area, Amazonian craton. *Brazilian Journal of Geology*, **52**(4):e20220017, 2022. https://doi.org/10.1590/2317-4889202220220017

M.J.B.M. and P.C.M. wrote the first draft of the manuscript and prepared the figures; M.L.V. improved the manuscript through corrections and suggestions. All of them did field work and sampling. R.A.A. provided U-Pb SHRIMP results. M.J.B.M. and M.L.V. prepared the final version.

Competing interests: the authors declare that they have no known competing financial interests or personal relationships that could have appeared to influence the work reported in this paper.

REFERENCES

Almeida F.F.M., Hasui Y., Brito Neves B.B., Fuck R.A. 1981. Brazilian structural provinces: an introduction. *Earth Science Review*, **17**(1-2), 1-29. https://doi.org/10.1016/0012-8252(81)90003-9

Alves C.L., Sabóia A.M., Martins E.G., Stropper J.L. 2010. *Folhas São José do Xingu e Comandante Fontoura, Escala 1:250.000*. Projeto Noroeste-Nordeste de Mato Grosso. Goiânia: Companhia de Pesquisas de Recursos Minerais – CPRM, 120 p.

Barros C.E.M., Macambira M.J.B., Barbey P., Scheller T. 2004. Dados isotópicos Pb-Pb em zircão (evaporação) e Sm-Nd do Complexo Granítico Estrela, Província Mineral de Carajás, Brasil: implicações petrológicas e tectônicas. *Revista Brasileira de Geociências*, **34**(4):531-38.

Besser M.L. 2012. *Origem e Evolução das rochas Paleoproterozoicas da área Rio Bacajá, Pará, Brasil*. MS dissertation. Curitiba: Universidade Federal do Paraná.

Bucher K., Grapes R. 2011. *Petogenesis of metamorphic rocks*. Berlin: Springer, 428 p.

Compston W., Williams I.S., Meyer C. 1984. U–Pb geochronology of zircons from lunar breccia 73217 using a sensitive high-resolution ion-microprobe. *Journal of Geophysical Research*, B98, 525-534. https://doi.org/10.1029/JB089iS02p0B525

Cordani U.G., Tassinari C.C.G., Kawashita K. 1984. A Serra dos Carajás como região limítrofe entre províncias tectônicas. *Ciências da Terra*, **9**, 6-11.

Cordani U.G., Tassinari C.C.G., Teixeira W., Basei M.A.S., Kawashita K. 1979. Evolução tectônica da Amazônia com base nos dados geocronológicos. In: Congresso de Geologia Chileno, Arica, **2**. *Actas…*, p. 137-148.

Corfu F., Hachar J.M., Hoskin P.W.O., Kinny P. 2003. Atlas of zircon textures. In: Hachar J.H., Hoskin P.W.O. (Eds.). *Reviews in Mineralogy and Geochemistry*. Washington, D.C.: The Mineralogical Society of America, **53**(1), p. 469-500.

Delor C., de Roever E.W.F., Lafon J.M., Lahondère D., Rossi P., Cocherie A., Guerrot C., Potrel A. 2003. The Bakhuis ultrahigh-temperature granulite belt (Suriname). II. Implications for late Transamazonian crustal stretching in a revised Guiana Shield framework. *Géologie de la France*, **2-4**, 207-230.

De Roever E.W.F., Lafon J.M., Delor C., Cocherie A., Rossi P., Guerrot C., Potrel A. 2003. The Bakhuis ultrahigh-temperature granulite belt (Suriname): I. petrological and geochronological evidence for a counterclockwise P–T path at 2.07–2.05 Ga. *Geology of France and Surrounding Areas*, **2-4**, 175-206.

De Roever E.W.F., Lafon J.M., Delor C., Guerrot C. 2015. Orosirian magmatism and metamorphism in Suriname: new geological constraints. In: Gorayeb P.S.S., Lima A.M.M. (Eds.). *Contribuições à Geologia da Amazônia*, **9**. Belém: SBG, p. 343-356.

Faraco M.T.L, Vale A.G., Santos J.O.S., Luzardo R., Ferreira A.L., Oliveira M.A., Marinho P.A.C. 2005. Levantamento Geológico da Região ao Norte da Província Carajás. In: Souza V., Horbe A.C. (Eds.). *Contribuições à Geologia da Amazônia*, **4**. Manaus: SBG, p. 32-44.

Feio G.R.L., Dall'Agnol R., Dantas E.L., Macambira M.J.B., Santos J.O.S., Althoff F.J., Soares J.E.B. 2013. Archean granitoid magmatism in the Canaã dos Carajás area: implications for crustal evolution of the Carajás province, Amazonian craton, Brazil. *Precambrian Research*, **227**, 157-185. https://doi.org/10.1016/j.precamres.2012.04.007

Fernandes C.M.D., Juliani C., Monteiro L.V.S., Lagler B., Misas C.M.E. 2011. High-K calc-alkaline to A-type fissure-controlled volcano- plutonism of the São Félix do Xingu region, Amazonian craton, Brazil: Exclusively crustal sources or only mixed Nd model ages? *Journal of South American Earth Sciences*, **32**(4), 351-368. https://doi.org/10.1016/j.jsames.2011.03.004

Gaudette H.E., Lafon J.M., Macambira M.J.B., Moura C.A.V., Scheller T. 1998. Comparasion of single filament Pb evaporation/ionization zircon ages with conventional U-Pb results: exemples from Precambrian of Brazil. *Journal of South American Earth Science*, **11**(4), 351-363. https://doi.org/10.1016/S0895-9811(98)00019-4

Grenholm M. 2019. The global tectonic context of the ca. 2.27-1.96 Ga Birimian Orogen – Insights from comparative studies, with implications for supercontinent cycles. *Earth-Science Reviews*, **193**, 260-298. https://doi.org/10.1016/j.earscirev.2019.04.017

Jorge João X.S., Vale A.G., Lobato T.A.M. 1987. *Folha SA.22-Y-D, Altamira, Estado do Pará*. Programa Levantamentos Geológicos Básicos do Brasil. Belém: CPRM/DNPM, 31 p.

Kober B. 1986. Whole grain evaporation for $^{207}Pb/^{206}Pb$ age investigations on single zircons using a double filament source. *Contributions to Mineralogy and Petrology*, **93**, 482-490. https://doi.org/10.1007/BF00371718

Ledru P., Johan V., Milési J.P., Tegyey M. 1994. Markers of the last stages of the Palaeproterozoic collision: Evidence for a 2 Ga continent involving circum South Atlantic provinces: *Precambrian Research*, **69**(1-4), 169-191. https://doi.org/10.1016/0301-9268(94)90085-X

Ludwig K.R. 2001. *Squid Version 1.03:* A User's Manual, 2. Berkeley: Berkeley Geochronology Center Special Publication, 18 p.

Ludwig K.R. 2003. *User's Manual for Isoplot/Ex version 3.00:* A Geochronology Toolkit for Microsoft Excel, 4. Berkeley: Berkeley Geochronological Center Special Publication, 70 p.

Macambira E.M.B., Ricci P.S.F. 2013. *Geologia e recursos minerais da Folha Tucuruí – SA.22-Z-C, Estado do Pará, Escala 1:250.000*. Belém: CPRM, 122 p.

Macambira E.M.B., Ricci P.S.F., Anjos G.C. 2016. *Folha Repartimento - SB.22-X. Mapa*. Escala 1:250.000. Belém: CPRM.

Macambira M.J.B., Lafon J.M. 1995. Geocronologia da Província Mineral de Carajás: Síntese dos dados e novos desafios. *Boletim do Museu Paraense Emilio Goeldi*, **7**, 263-287.

Macambira M.J.B., Pinheiro R.V.L., Armstrong R.A. 2007. A fronteira Arqueano-Paleoproterozoico no SE do Cráton Amazônico; Abrupta no tempo, suave na tectônica? In: Simpósio de Geologia da Amazônia, Porto Velho, 10. *Boletim de Resumos*... Porto Velho: SBG, p. 97-100.

Macambira M.J.B., Vasquez M.L., Silva D.C.C., Galarza M.A., Barros C.E.M., Camelo J.F. 2009. Crustal growth of the central-eastern Paleoproterozoic Bacajá domain, SE Amazonian craton: juvenile accretion vs. reworking. *Journal of the South American Earth Sciences*, **27**(4), 235-246. https://doi.org/10.1016/j.jsames.2009.02.001

Machado N., Lindenmayer Z., Krogh T.E., Lindenmayer D. 1991. U-Pb geochronology of archaean magmatism and basement reactivation in the Carajás area, Amazon shield, Brazil. *Precambrian Research*, **49**(3-4), 329-354. https://doi.org/10.1016/0301-9268(91)90040-H

Melo G.H.C., Monteiro L.V.S., Xavier R.P., Moreto C.P.N., Santiago E.S.B., Dufrane S.A., Aires B., Santos A.F.F. 2016. Temporal evolution of the giant Salobo IOCG deposit, Carajás province (Brazil): Constraints from paragenesis of hydrothermal alteration and U-Pb geochronology. *Mineralium Deposita*, **52**, 709-732. https://doi.org/10.1007/s00126-016-0693-5

Moreto C.P.N., Monteiro L.V.S., Xavier R.P., Amaral W.S., Santos T.J.S., Juliani C., Souza Filho C.R. 2011. Mesoarchean (3.0 and 2.86 Ga) host rocks of the iron oxide–Cu–Au Bacaba deposit, Carajás Mineral Province: U–Pb geochronology and metallogenetic implications. *Mineralium Deposita*, **46**, 789-811. https://doi.org/10.1007/s00126-011-0352-9

Nadeau S., Chen W., Reece J., Lachhman D., Ault R., Faraco M.T.L., Fraga L.M., Reis N.J., Betiollo L.M. 2013. Guyana: the Lost Hadean crust of South America? *Brazilian Journal of Geology*, **43**(4), 601-606. https://doi.org/10.5327/Z2317-48892013000400002

Olszewski W.J., Wirth K.R., Gibbs A.K., Gaudette H.E. 1989. The age, origin and tectonics of the Grão Pará Group and associated rocks, Serra dos Carajás, Brazil: Archean continental Volcanism and rifting. *Precambian Research*, **42**(3-4), 229-254. https://doi.org/10.1016/0301-9268(89)90013-2

Passchier C.W., Trouw R.A.J. 2005. *Microtectonics*. 2ª ed. Berlin: Springer, 366 p.

Rosa-Costa L.T., Lafon J.M., Cocherie A., Delor C. 2008. Electron microprobe U-Th-Pb monazite dating of the Transamazonian metamorphic overprint on Archean rocks from the Amapá block, southeastern Guiana shield, northern Brazil. *Journal of the South American Earth Sciences*, **26**(4), 445-462. https://doi.org/10.1016/j.jsames.2008.05.007

Rosa-Costa L.T., Lafon J.M., Delor C. 2006. Zircon geochronology and Sm–Nd isotopic study: further constraints for the Archean and Paleoproterozoic geodynamic evolution of the southeastern Guiana Shield, north of Brazil. *Gondwana Research*, **10**(3-4), 277-300. https://doi.org/10.1016/j.gr.2006.02.012

Rosa-Costa L.T., Patrick Monié P., Lafon J.M., Arnaud N.O. 2009. ^{40}Ar–^{39}Ar geochronology across Archean and Paleoproterozoic terranes from southeastern Guiana Shield (north of Amazonian Craton, Brazil): Evidence for contrasting cooling histories. *Journal of the South American Earth Sciences*, **27**(2-3), 113-128. https://doi.org/10.1016/j.jsames.2008.08.010

Santos J.O.S. 2003. Geotectônica do Escudo das Guianas e Brasil central. In: Bizzi L.A., Schobbenhaus C., Vidotti R.M., Gonçalves J.H. (Eds.). *Geologia, tectônica e recursos minerais do Brasil*. Brasília, CPRM, **4**, p. 169-226.

Santos J.O.S., Hartmann L.A., Gaudette H.E., Groves D.I., Mcnaughton N.J. Fletcher I.R. 2000. A new understanding of the provinces of the Amazon craton based on integration of field and U-Pb and Sm-Nd geochronology. *Gondwana Research*, **3**(4), 453-488. https://doi.org/10.1016/S1342-937X(05)70755-3

Santos M.V., Tassinari C.C.G., Souza Filho E.E., Teixeira W., Ribeiro A.C.O., Payolla B., Vasconi A. 1988. Litoestratigrafia das rochas precambrianas da bacia do médio rio Xingu, Altamira, Pará. In: Congresso Latino-Americano de Geologia, 7, Belém. *Anais*… Belém: SBG, p. 363-377.

Sawyer E.W. 2008. Working with migmatites: nomenclature for the constituent parts. *In*: Sawyer E.W. (Ed.). *Working with migmatites*. Canada: Mineralogical Association of Canada Short Course Series, **8**, p. 1-28.

Semblano F.R.D., Pereira N.C.S., Vasquez M.L., Macambira M.J.B. 2016. Novos dados geológicos e isotópicos para o Domínio Iriri-Xingu, Província Amazônia Central: implicações para a idade do Grupo Iriri. *Geologia USP. Série Científica*, **16**(3), 19-38. https://doi.org/10.11606/issn.2316-9095.v16i3p19-38

Stacey J.S., Kramers J.D. 1975. Approximation of terrestrial lead isotope evolution by a two stages model. *Earth and Planetary Science Letters*, **26**(2), 207-221. https://doi.org/10.1016/0012-821X(75)90088-6

Tassinari C.C.G., Bettencourt J.S., Geraldes M.C., Macambira M.J.B. Lafon J.M. 2000. The Amazonian Craton. In: Cordani U.G., Milani E.J., Filho A.T., Campos D.A. (Eds.). *Tectonic Evolution of the South America*. Rio de Janeiro: SBG, p. 41-95.

Tassinari C.C.G., Macambira M.J.B. 1999. Geochronological provinces of the Amazonian Craton. *Episodes*, **22**(3), 174-182. https://doi.org/10.18814/epiiugs/1999/v22i3/004

Tassinari C.C.G., Macambira M.J.B. 2004. A evolução tectônica do Cráton Amazônico. In: Mantesso Neto V., Bartorelli A., Carneiro C.D.R., Neves B.B.B. (Eds.). *Geologia do continente Sul-americano:* evolução da obra de Fernando Flávio Marques de Almeida. São Paulo: Beca, p. 471-485.

Tassinari C.C.G., Munhá J.M.V., Teixeira W., Palácios T., Nutman A.P., Sousa C.S., Santos A.P., Calado B.O. 2004. The Imataca Complex, NW Amazonian Craton, Venezuela: crustal evolution and integration of geochronological and petrological cooling histories. *Episodes*, **27**(1), 3-12. https://doi.org/10.18814/epiiugs/2004/v27i1/002

Tavares F.M., Trouw R.A.J., Silva C.G.G. Justo A.P., Olivera J.K.M. 2018. The multistage tectonic evolution of the northeastern Carajás Province, Amazonian Craton, Brazil: Revealing complex structural patterns. *Journal of South American Earth Sciences*, **88**, 238-252. https://doi.org/10.1016/j.jsames.2018.08.024

Teixeira W., Tassinari C.C.G., Cordani U.G., Kawashita K. 1989. A review of the geochronology of the Amazonian Craton: tectonic implications. *Precambrian Research*, **42**(3-4), 213-227. https://doi.org/10.1016/0301-9268(89)90012-0

Toledo P.I.F., Moreto C.P.N., Xavier R.P., Gao J., Matos J.H.S.N., Melo G.H. 2019. Multistage Evolution of the Neoarchean (ca. 2.7 Ga) Igarapé Cinzento (GT-46) Iron Oxide Copper-Gold Deposit, Cinzento Shear Zone, Carajás Province, Brazil. *Economic Geology*, **114**(1), 2-34. https://doi.org/10.5382/econgeo.2019.4617

Vasquez M.L., Macambira M.J.B., Armstrong R.A. 2008a. Zircon geochronology of granitoids from the western Bacajá domain, southeastern Amazonian craton, Brazil: Neoarchean to Orosirian evolution. *Precambrian Research*, **161**(3-4), 279-302. https://doi.org/10.1016/j.precamres.2007.09.001

Vasquez M.L., Macambira M.J.B., Armstrong R.A. 2014. High grade metamorphism constrained by U-Pb SHRIMP ages: An example of Bacajá domain, Amazonian craton, Brazil. In: South American Symposium of Isotope Geology, **9.** *Abstracts*… São Paulo: CPGeo-USP/SBG.

Vasquez M.L., Macambira M.J.B., Galarza M.A. 2005. Granitóides Transamazônicos da Região Iriri-Xingu, Pará - Novos dados geológicos e geocronológicos. In: Souza V., Horbe A.C. (Eds.). *Contribuições à Geologia da Amazônia*. Manaus: SBG, **4**, p. 16-31.

Vasquez M.L., Rosa-Costa L.T., Silva C.M.G., Klein E.L. 2008b. Compartimentação tectônica. In: Vasquez M.L., Rosa Costa L.T. (Eds.). *Geologia e Recursos Minerais do Estado do Pará:* Sistema de Informações Geográficas – SIG: Texto explicativo dos mapas geológico e tectônico e de recursos minerais do Estado do Pará. Escala 1:1.000.000. Belém: CPRM, p. 39-112.

Vasquez M.L., Sousa C.S., Carvalho J.M.A. 2008c. *Mapa Geológico e de Recursos Minerais do Estado do Pará*. Escala 1:1.000.000. Programa Geologia do Brasil (PGB). Integração, Atualização e Difusão de Dados da Geologia do Brasil. Mapas Geológicos Estaduais em SIG. Belém: CPRM.

Williams I.S. 1998. U–Th–Pb geochronology by ion microprobe. In: McKibben M.A., Shanks III W.C., Rydley W.I. (Eds.). *Applications of microanalytical techniques to understanding mineralizing processes*. El Paso: Society of Economic Geologists, Reviews in Economic Geology, **7**, p. 1-35. https://doi.org/10.5382/Rev.07